HHS Public Access

Author manuscript

Oncogene. Author manuscript; available in PMC 2017 May 21.

Published in final edited form as:

Oncogene. 2017 April 06; 36(14): 1939–1951. doi:10.1038/onc.2016.405.

Human Pot1 OB-fold mutations unleash rampant telomere instability to initiate tumorigenesis

Peili Gu[1], **Yang Wang**[1], **Kamlesh K. Bisht**[2], **Ling Wu**[3], **Lidiya Kukova**[1], **Eric M. Smith**[2], **Yang Xiao**[4], **Susan Bailey**[5], **Ming Lei**[6], **Jayakrishnan Nandakumar**[2], and **Sandy Chang**[1,7,8,*]

[1]Department of Laboratory Medicine, Yale University School of Medicine, 330 Cedar St., New Haven, CT 06520, USA

[2]Department of Molecular, Cellular, and Developmental Biology, University of Michigan, Ann Arbor, MI 48109, USA; [2]Program in Chemical Biology, University of Michigan, Ann Arbor, MI 48109, USA

[3]Department of GI Medical Oncology, U.T. MD Anderson Cancer Center, 1515 Holcombe Blvd, Houston, TX 77030, USA

[4]Section of Hematology-Oncology, Department of Medicine and Molecular and Cellular Biology, Baylor College of Medicine, One Baylor Plaza, Houston, TX 77030, USA

[5]Department of Environmental & Radiological Health Sciences, Colorado State University, Fort Collins, CO 80523-1618, USA

[6]National Center for Protein Science Shanghai, State Key Laboratory of Molecular Biology, Institute of Biochemistry and Cell Biology, Shanghai Institutes for Biological Sciences, Chinese Academy of Sciences, Shanghai, China

[7]Department of Pathology, Yale University School of Medicine, 330 Cedar St., New Haven, CT 06520, USA

[8]Department of Molecular Biophysics and Biochemistry, Yale University School of Medicine, 330 Cedar St., New Haven, CT 06520, USA

Abstract

Chromosomal aberrations are a hallmark of human cancers, with complex cytogenetic rearrangements leading to genetic changes permissive for cancer initiation and progression. Protection of Telomere 1 (POT1) is an essential component of the shelterin complex and functions

*Correspondence: Sandy Chang, Yale University School of Medicine, Dept. of Laboratory Medicine, BML 462, 333 Cedar St., New Haven, CT 06520, schang@yale,edu.

Author Contributions

SC and ML conceived the project. SC, PG, KKB and JN designed the experiments. PG, YW performed all the telomere biology and transplantation experiments. LW and YX generated the breast cancer mouse model and performed tumor analysis. KKB and EMS performed the *in vitro* telomerase assay. SB analyzed the cytogenetics data. PG, JN, ML and SC analyzed and interpreted the data, composed the figures and SC wrote the paper.

Competing Financial Interests

The authors declare no competing financial interests.

to maintain chromosome stability by repressing the activation of aberrant DNA damage and repair responses at telomeres. Sporadic and familial mutations in the oligosaccharide-oligonucleotide (OB) folds of POT1 have been identified in many human cancers, but the mechanism underlying how hPOT1 mutations initiate tumorigenesis has remained unclear. Here we show that the human POT1's OB-folds are essential for the protection of newly replicated telomeres. Oncogenic mutations in hPOT1 OB-fold fail to bind to ss telomeric DNA, eliciting a DNA damage response at telomeres that promote inappropriate chromosome fusions via the mutagenic alternative non-homologous end joining (A-NHEJ) pathway. hPOT1 mutations also result in telomere elongation and the formation of transplantable hematopoietic malignancies. Strikingly, conditional deletion of both *mPot1a* and *p53* in mouse mammary epithelium resulted in development of highly invasive breast carcinomas and the formation of whole chromosomes containing massive arrays of telomeric fusions reminiscent of chromothripsis. Our results reveal that hPOT1 OB-folds are required to protect and prevent newly replicated telomeres from engaging in A-NHEJ mediated fusions that would otherwise promote genome instability to fuel tumorigenesis.

Introduction

The proper maintenance of a stable genome is essential for an individual's health and is paramount for faithful transmission of genetic information to future generations. One important mechanism that protects against the acquisition of an unstable genome is the proper function of telomeres, DNA-protein complexes that cap the ends of all eukaryotic chromosomes[1]. Mammalian telomeres are composed of repetitive TTAGGG DNA sequences synthesized by the enzyme telomerase which together with a number of telomere-specific binding proteins form the shelterin complex to safeguard telomeres from inappropriately activating DNA damage responses (DDR) [2, 3]. Three sequence specific telomere binding proteins are recruited to chromosomal ends: the duplex telomere repeat factors TRF1 and TRF2/RAP1, and the single-stranded (ss) telomere DNA binding protein Protection of Telomere 1 (POT1). POT1 forms a heterodimer with TPP1, and this heterodimer acts to regulate telomerase access to telomeres [4–9]. TPP1 directly recruits telomerase to telomeres to enable telomere elongation, while POT1 negatively regulates telomere length by modulating telomerase access to telomeres through physical interaction of its highly conserved oligonucleotide/oligosaccharide binding (OB) folds with the ss G-overhang [10–12]. The mouse genome encodes two *mPot1* genes, *mPot1a* and *mPot1b*, while a single human *hPot1* is postulated to possess the functions of both mouse proteins [13–16]. Removal of mPOT1a, hPOT1 (and to a lesser extent mPot1b) results in activation of a potent ATR-dependent DDR, marked by recruitment of replication protein A (RPA), the sensor of the ATR pathway, to telomeres. This DDR also promotes activation of downstream signaling kinases, including Chk1, and marks dysfunctional telomeres as double-stranded breaks (DSBs)[17–20]. mPOT1b's main function is to inhibit 5′ nucleolytic processing of the telomeric C-strand, limiting the length of the 3′ ss telomeric overhang [13, 21]. Highly proliferative mouse cells lacking *mPot1b* generate long stretches of ss telomeric DNA that activates p53-dependent DNA damage checkpoint responses and diminished stem cell proliferation, consequences of which include bone marrow failure and compromised organismal lifespan [13, 22, 23]. These results reveal essential roles for POT1 proteins in

preventing the inappropriate activation of the ATR-mediated, p53-dependent DNA damage signaling at telomeres.

POT1 proteins are also required to prevent inappropriate repair of dysfunctional telomeres. Activation of the ATR kinase, and generation of 3′ ss overhangs, are both essential to promote alternative, non-homologous end joining (A-NHEJ)-mediated repair of mouse telomeres devoid of *Pot1a/b* [24–28]. A-NHEJ is a microhomology based error-prone repair pathway that fosters the generation of gross chromosomal abnormalities, including large deletions, insertions and translocations, thereby increasing genome instability [27, 29, 30]. This pathway has emerged as the primary DNA repair pathway in several human cancers [31, 32]. We have shown previously that deletion of *mPot1a* and *mPot1b* in conditional knockout mouse models activates a potent p53-dependent DDR, resulting in cellular senescence and apoptosis [14, 22, 2333]. In the absence of a functional p53 pathway, loss of mPOT1a or mPOT1b promotes end-to-end chromosome fusions and cancer formation, suggesting that POT1 proteins are critically important for preventing the onset of tumor promoting genomic instability. In accord with our mouse studies, whole genome sequencing efforts have revealed that recurrent *hPot1* mutations are present at high frequencies in patients with chronic lymphocytic leukemia (CLL) and familial melanomas (FM) [34–37]. These results highlight the importance of hPOT1 in maintaining genome stability to prevent the onset of tumorigenesis. However, it is unclear how hPOT1 exerts these critical protective functions.

In our current study, we investigated how hPOT1 OB-fold mutations promote tumorigenesis. We demonstrate that mutant hPOT1 elicits a DDR at telomeres that is repaired through the error-prone A-NHEJ DNA repair pathway. When transduced into hematopoietic stem cells, mutant hPOT1 initiates transplantable myeloid malignancies and increased telomere lengths during long term culture. Conditional deletion of both *mPot1a* and *p53* from mouse mammary epithelium resulted in development of highly invasive breast tumors that were highly genomically unstable, bearing impressive arrays of telomeric signals indicative of multiple breakage-fusion-bridge (BFB) cycles. Finally, we show that the OB-folds of hPOT1 are required to protect newly replicated telomeres from fusion. Our results reveal important roles for hPOT1 OB-fold mutations in promoting both genome instability and increased telomere elongation to favor tumor initiation.

Results

hPot1 OB-fold mutations induce a DNA damage response at telomeres

Recent whole-genome and exome sequencing have identified recurrent *hPot1* mutations in ~9% of the most aggressive form of CLL, making *hPot1* the second most frequently mutated gene to date identified in CLL [35, 36]. In familial melanoma (FM), *hPot1* is also the second most frequently mutated, high penetrance gene reported thus far, representing ~30% of all FM cases[36, 37]. hPOT1 is thus the first shelterin component found to be mutated in diverse human cancers. CLL and FM hPOT1 somatic mutations cluster primarily within the two OB-folds and are predicted to disrupt phylogenetically conserved amino acid residues (Figure 1A and Supplemental Figure 1A). For example, crystal structure analyses revealed that two residues mutated in cancer, Tyr89 and Gln94, interact with the fourth G residue in the TTA_3G_4GG telomeric repeat [11]. The aromatic phenol ring of Tyr89 stacks with G4 and

A3, providing non-specific interactions. In contrast, the side chain of Gln94 mediates two hydrogen-bonding interactions with G4, thus specifically recognizing a G in this position. Mutating these residues to other amino acids is predicted to interfere with POT1 OB-fold's hydrogen bonding with telomeric DNA (Figure 1B and Supplemental Figure 1B). To test this hypothesis, we used site-directed mutagenesis to generate *hPot1* CLL and FM point mutations Y36N, Y89C, Y223C, and S270N. Because Q94 is a shared amino acid residue between both CLL and FM, we mutated it to an alanine, which is predicted to abolish hPOT1's interaction with G4 (Figure 1B). We first examined whether these hPOT1 OB-fold mutants are able to bind to ss $(TTAGGG)_4$ oligos *in vitro*. Four hPOT1 mutants displayed either markedly reduced binding (S270N), or were completely unable to bind to ss telomeric oligos (Y89C, Q94A, Y223C, S270N) (Figure 1C). The $hPOT1^{Y36N}$ mutant bound to ss telomeric DNA with high affinity (Figure 1C), and behaved like WT hPOT1 in subsequent telomeric assays (data not shown). These results demonstrate that tumorigenic hPOT1 OB-fold mutations disrupt binding to ss telomeric DNA *in vitro*, supporting the conclusions drawn from previous studies [34–36].

Localization of both mouse and human POT1 to telomeres in cells requires interaction with its heterodimeric partner TPP1, while the POT1 OB-folds appear dispensable for *in vivo* telomere localization [13–15, 38]. To determine whether OB-fold mutations disrupted binding to TPP1, we subjected the HA-tagged hPOT1 mutants to immunoprecipitation (IP) experiments with Flag-hTPP1. We found that all hPOT1 OB-fold mutants interact with hTPP1 as robustly *in vitro* as WT hPOT1, indicating that these mutations do not disrupt hPOT1's interaction with hTPP1 (Figure 1C). In addition, stabilization of hPOT1 requires binding to hTPP1, since WT hPOT1 is unstable in the presence of the $hTPP1^{\Delta RD}$ mutant unable to bind to hPOT1 (Figure 1C). Immunofluorescence microscopy confirmed that all hPOT1 OB-fold mutants are stably expressed and readily localized to telomeres in both U2OS and IMR90 cells (Supplemental Figures 2A–2C and 3A–3C). Since mammalian POT1 proteins function to repress a DDR at telomeres, we next asked whether the hPOT1 OB-fold mutations abolish this function, using the dysfunctional telomere induced DNA damage foci (TIF) assay to monitor recruitment of DNA damage marker γ-H2AX to telomeres in both U2OS and IMR90 cell lines. Greater than 5 TIFs per cell were observed in 35–40% of U2OS cells expressing the *hPot1* OB-fold mutants examined, almost as many as those observed in cells expressing the dominant negative mutant $TPP1^{\Delta RD}$ (Figures 1D, 1E, Supplemental Figures 2A and 2D). TIFs were also observed in immortalized IMR90 cells expressing hPOT1 mutants, although not at the levels observed in U2OS cells (Supplemental Figure 3A and 3D). Expression of hPOT1 OB-fold mutations resulted in the generation of end-to-end chromosomal fusions in 1.5–2.5% of all IMR90 chromosomes scored; telomeric signals was present at some sites of fusion (Figures 1F, 1G). Taken together, these results confirm previous findings in human tumors that hPOT1 OB-fold mutations activate DNA damage signaling at telomeres [35–37]. While fusions were rare in human tumors, our results suggest that inappropriate repair of telomeres lacking functional hPOT1 OB-folds promoted formation of fused chromosomes.

hPOT1 OB-fold mutants promote A-NHEJ-mediated chromosomal fusions

hPot1 mutations in CLL and FM are heterozygous mutations. To determine whether mutant hPOT1 proteins function as a dominant negative and require the presence of the WT hPOT1 allele to promote chromosome fusions, we generated *CAG-Cre^{ER}-mPot1a$^{F/F}$; mPot1b$^{-/-}$* mouse embryo fibroblasts (MEFs), which permitted 4-hydroxytamoxafen (4-HT)-mediated activation of Cre recombinase for efficient depletion of the endogenous *mPot1a* allele to generate a *mPot1a/b* null background. 4-HT mediated depletion of the endogenous mPOT1a protein initiated a robust ATR-dependent DDR, marked by phosphorylation of Chk1 and RPA (Supplemental Figure 4A). Reconstitution of *CAG-Cre^{ER}-mPot1a$^{\Delta/\Delta}$; mPot1b$^{-/-}$* MEFs with empty vector resulted in robust TIF formation involving ~40% of all cells examined. Expression of WT *mPot1a* repressed TIF formation to background levels (~5%), while elevated TIF formation was observed in over 60% of cells expressing OB-fold mutants *mPot1a^{F62A}* and *mPot1b^{F62A}*, or *TPP1$^{\Delta RD}$* (Figure 2A, Supplemental Figure 4B). Expression of WT *mPot1b* in this system did not appreciably rescue TIF formation, suggesting that in mouse cells, mPOT1a is primarily responsible for repression of a DDR at telomeres (Figure 2A). This observation is consistent with the finding that the DDR is not prominent in untreated *CAG-Cre^{ER}-mPot1a$^{F/F}$; mPot1b$^{-/-}$* MEFs (Supplemental Figures 4A, 5A) [21]. Expression of all *hPot1* alleles together with *hTpp1* in *CAG-Cre^{ER}-mPot1a$^{\Delta/\Delta}$; mPot1b$^{-/-}$* MEFs promoted efficient localization of hPOT1 to mouse telomeres (Supplemental Figure 4C) [16]. We found that only expression of WT *hPot1* was able to repress TIF formation, while 60% of cells expressing all *hPot1* OB-fold mutants examined display increased TIF formation (Figure 2A). To examine the role of OB-fold mutants in repressing a DDR at telomeres, we utilized the mPOT1^{F62A} OB-fold mutant, which we have previously shown to disrupt ss telomeric DNA binding and elicits a potent DDR at telomeres (Supplemental Figures 1A, 1B) [11, 14]. *mPot1a^{F62A}* and *mPot1b^{F62A}* expression in *CAG-Cre^{ER}-mPot1a$^{\Delta/\Delta}$; mPot1b$^{-/-}$* MEFs was unable to repress ATR-dependent DDR, and similar to the *hPot1* OB-fold mutants, also generated chromosome-type and chromatid-type fusions involving ~10% of all chromosome ends, some with and some without telomeres at fusion sites. In addition, sister chromatid fusions (sister unions), a hallmark of telomeres devoid of functional POT1, were also observed (Figure 2B, Supplemental Figures 5A, 5B). Expression of WT *mPot1a* and *mPot1b* repressed activation of the DDR (Supplemental Figure 5A). WT *mPot1a*, *mPot1b* and *hPot1* also reduced chromosome fusion frequencies to background levels (Supplemental Figure 5B). These results suggest that while mPOT1b plays a reduced role in preventing activation of a DDR at telomeres, it is required to prevent inappropriate repair of telomere ends. In addition, our data suggest that hPOT1 OB-fold mutants do not require the presence of WT hPOT1 to render telomeres dysfunctional; these mutants are fully capable of eliciting a DDR that initiates aberrant DNA repair and the generation of chromosome fusions.

Uncapped telomeres can be repaired either by the error-prone non-homologous end joining (NHEJ) or the error-free homologous recombination (HR) repair pathways. NHEJ can proceed either by the Classic, Lig4-dependent pathway (C-NHEJ), or by the Alternative, LIG 4-independent, PARP1-dependent NHEJ (A-NHEJ) pathway [27, 39]. We have previously shown that mPOT1a/b are required to protect the ss G-overhang from engaging in A-NHEJ mediated DNA repair [24]. To determine whether the chromosome fusions observed upon

expression of the hPOT1 mutants are generated by A-NHEJ-mediated repair, we expressed *mPot1a*^{F62A} and *mPot1b*^{F62A} in *Ku70*$^{-/-}$ MEFs defective in C-NHEJ, but not A-NHEJ-mediated DNA repair [40, 41]. TIFs and end-to-end chromosomal fusions were both prominent in *Ku70*$^{-/-}$ MEFs expressing both *mPot1a* and *mPot1b* mutants (Figure 2C, Supplemental Figures 6A, 6B). PNA-telomere FISH analysis revealed that expression of *hPot1* OB-fold mutants along with *hTpp1* in *Ku70*$^{-/-}$ MEFs also yielded increased numbers of TIFs and end-to-end chromosome fusions both with and without telomeric signals at fusion sites, as well as sister chromatid fusions (Figure 2D, Supplemental Figure 6B). These results indicate that expression of *mPot1a/b* and *hPot1* OB-fold mutants promote A-NHEJ-mediated DNA repair. In support of this notion, inhibition of the A-NHEJ pathway following treatment with the PARP1 inhibitor VIII PJ34 resulted in an ~50% reduction in the number of chromosome fusions in both *Ku70*$^{-/-}$ MEFs and IMR90 cells expressing *mPot1a/b* or *hPot1* OB-fold mutations, respectively (Figures 2E, 2F).

Most *hPot1* OB-fold mutations inhibit telomerase activity *in vitro* but promote telomere elongation *in vivo*

hPOT1 has been shown to inhibit telomerase activity *in vitro* by competing for access to the 3′ end of G-rich ss telomeric DNA[42]. Since hPOT1 OB-fold mutants interact poorly with ss telomeric DNA (Figure 1C), we hypothesized that mutations in the hPOT1 OB-fold might enable increased telomerase access to the 3′ G-rich overhang, promoting telomere elongation. To test this hypothesis, we performed direct telomerase primer extension assays using HEK 293T cells transiently co-expressing telomerase and either WT or mutant hPOT1. We observed the characteristic decrease of telomerase activity in the presence of WT hPOT1 (Figure 3A). In addition, we observed that the hPOT1 F62A, Q94A, Y223C, and S270N mutants were all as efficient as WT hPOT1 in inhibiting telomerase activity. However, we observed a ~10% and ~60% defect in telomerase inhibition in the presence of hPOT1^{Y36N} and hPOT1^{Y89C}, respectively, suggesting that at least *in vitro* the DNA-binding defects of these two mutants correlate with their diminished ability to inhibit telomerase (Figures 3A, 3B). The differences in the abilities of the hPOT1 mutants to inhibit telomerase do not arise from differences in hPOT1 expression, since hPOT1 mutant expression is uniform across the various transfections (Figure 3C).

We next asked whether expression of hPOT1 OB-fold mutants affected telomere length maintenance *in vivo*, using the telomerase positive HT1080 cells. We found that upon serial passaging, expression of all *hPot1* mutants resulted in progressive telomere elongation, from an average telomere length of ~4.5 kb to 9.5 kb over 75 population doublings (Figure 3D, Supplemental Figures 7A, 7B). As a negative control, telomere elongation was not observed in HT1080 cells expressing vector control, the *hTpp1* OB^{WT} construct [43], nor in serially passaged IMR90 cells expressing WT *hPot1* or mutants (Supplemental figures 7B–7D). These findings suggest that while the majority of *hPot1* OB-fold mutants were able to inhibit telomerase activity in an *in vitro* assay, in long term passaging experiments all displayed increased telomere length elongation similar to the *hPot1* mutant human tumors [35–37] or cells expressing the *hPot1*$^{\Delta OB}$ mutant which is unable to negatively regulate telomerase access to telomeres[44].

Finally, we asked whether *hPot1* mutations impacted upon the ability for telomerase to be recruited to telomeres by performing a modified immunofluorescence/FISH-based telomerase recruitment assay [12]. HeLa cells expressing the catalytic subunit of telomerase (TERT), the RNA subunit of telomerase (TR) and either WT or mutant *hPot1* were fixed and stained for telomeres and TR. While localization of TR to telomeres was reduced when TPP1 was not co-expressed in this assay, we found that endogenous TPP1 was sufficient to permit TR localization to 3–4 telomeres in the majority of cells examined. The number of TR positive foci per cell, and the percentage of telomeres co-localizing with TR, was similar in cells expressing either WT or mutant *hPot1* (Figure 3E, Supplemental Figures 7C, 7D). These results suggest that hPOT1 OB-fold mutations do not impact upon telomerase recruitment to telomeres.

Reconstitution of *hPot1^{Y223C}* expressing hematopoietic cells in SCID mice promotes the formation of transplantable hematopoietic malignancy

Our data support the notion that hPOT1 OB-fold mutants promote both genomic instability through loss of ATR-mediated DDR repression and telomere elongation via loss of telomerase regulation, both of which are causal for cancer development. To further determine how these mutations might promote tumorigenesis, we analyzed the CLL *hPOT1^{Y223C}* mutation in greater detail, since this recurrent mutation has been identified in several CLL patients [35]. We generated *MSCV- hPot1^{Y223C}-GFP* and *MSCV- hPot1^{WT}-GFP* retroviral vectors, and along with *hTpp1*, transduced them independently into murine *p53$^{+/-}$* fetal liver cells to investigate the impact of mutant *hPot1* expression in the hematopoietic system. Both WT hPOT1 and hPOT1^{Y223C} readily localized to telomeres of mouse fetal liver cells, but only hPOT1^{Y223C} initiated TIF formation (Figures 4A, 4B, Supplemental Figure 8A). Retrovirally infected fetal liver cells were injected into lethally irradiated SCID mice, and serial bleeds were performed to monitor GFP expression as a marker of BM engraftment. In 4/8 recipient mice, hPOT1^{Y223C}-GFP levels increased steadily post transplantation, while hPOT1^{WT}-GFP levels declined, suggesting that engraftment of hematopoietic cells expressing *hPOT1^{Y223C}-GFP* conferred a positive selective advantage to irradiated recipients (Figure 4C). Bone marrow (BM) cells isolated from stably engrafted mice after 30 weeks displayed end-to-end chromosomal fusions, and RT-PCR analysis revealed that these cells express the *hPot1^{Y223C}* transgene (Figures 4D, 4E, Supplemental Figure 8B). Histological analysis revealed that myeloid dysplasia was prominent in the BM of mice expressing *hPot1^{Y223C}-GFP*, with increased number of blasts, promyelocytes, myelocytes and metamyelocytes observed (Figure 4F). FACS analysis revealed a significant increase in the CD11b^{+} population (Figure 4G), consistent with myeloid expansion. Examination of the liver and spleen revealed extensive CD11b^{+} liver infiltration (Supplemental Figure 8C). Importantly, this myeloid malignancy was transplantable into a second round of recipient SCID mice, forming CD11b^{+} liver and splenic metastatic infiltrates (Figure 4H). Taken together, these results suggest that expression of mutant *hPot1^{Y223C}* in hematopoietic cells promotes development of transplantable myeloid malignancy.

Deletion of *mPot1a* and *p53* in the breast promotes the development of invasive breast carcinomas

In addition to CLL and FM, our recent analysis of the TCGA database revealed that numerous missense somatic *hPot1* mutations involving highly conserved amino acids in the hPOT1 OB-folds are present in diverse human cancers, including cancers in solid tumors including breast, brain, lung, bladder, stomach and cervix (Supplemental Figure 9). Since these mutations map to conserved amino acid residues throughout the OB-folds, it is likely that they also disrupt hPOT1 function. To understand mechanistically how POT1 protects telomeres to prevent initiation of solid tumors, we generated *MMTV-Cre; mPot1a*$^{F/F}$ mice to conditionally delete endogenous *mPot1a* in a temporal manner in mouse mammary epithelium. All *MMTV-Cre; mPot1a*$^{F/F}$ mice developed breast cancer after 24 months of age. Interestingly, 100% of these breast cancers lost p53 function, suggesting that deletion of *mPot1a* alone is insufficient to promote tumorigenesis. We hypothesized that breast cancer formation in this model system requires loss of both *mPot1a* and *p53*. To test this hypothesis, we generated *MMTV-Cre; mPot1a*$^{F/F}$*; p53*$^{F/+}$ and *MMTV-Cre; mPot1a*$^{F/F}$*; p53*$^{F/F}$ mice. 100% of *MMTV-Cre; mPot1a*$^{\Delta/\Delta}$*; p53*$^{F/+}$ mice developed breast cancer, with a median tumor latency of 17 months, while 100% of *MMTV-Cre; mPot1a*$^{\Delta/\Delta}$*; p53*$^{F/F}$ mice developed breast cancers by 8.4 months of age (Figure 5A). Histological analysis revealed that the majority of these tumors were invasive breast adenocarcinomas (Figure 5B) that stained positively to antibodies against cytokeratin markers CK5, 8 and 14 but not against ER-alpha (Figure 5C). To further examine the p53 status of these tumors, we generated breast tumor cell lines and exposed them to 10 Gy ionizing radiation (IR). While normal mouse mammary epithelial cells were able to induce expression of both p53 and its downstream target p21 following IR exposure, p53 or p21 induction was not observed in any of the tumor cell lines, confirming loss of p53 function (Figure 5D). Compared to telomere lengths observed in a *mPot1a*$^{+/+}$*; p53*$^{-/-}$ lymphoma, TRF Southern analysis revealed that total telomere length was significantly increased and highly heterogeneous in all *MMTV-Cre; mPot1a*$^{\Delta/\Delta}$*; p53*$^{\Delta/\Delta}$ tumors examined (Figure 5E). Finally, TIF formation was also increased in these breast tumors (Figure 5F). Taken together, these results suggest that compromised mPOT1a function, coupled with loss of p53, promotes formation of invasive breast adenocarcinomas.

MMTV-Cre; Pot1a$^{\Delta/\Delta}$*; p53*$^{\Delta/\Delta}$ breast tumors display massive telomere-DSB amplifications

Compared to metaphase chromosome spreads derived from *MMTV-Cre; p53*$^{\Delta/\Delta}$ lymphoma, PNA-telomere FISH revealed that ~30% of *MMTV-Cre; Pot1a*$^{\Delta/\Delta}$*; p53*$^{\Delta/\Delta}$ breast tumors exhibit massive telomeric amplifications involving one, or at most a few, chromosomes. Extensive blocks of interstitial telomeric signals (ITS) encompassed large portions of individual chromosomes – or even entire chromosomes (Figure 6A, Supplemental Figure 10). Such a striking telomeric phenotype has not been previously described in tumors from other mouse models of telomere dysfunction. Further, these cytogenetic anomalies were present in all metaphases examined, suggestive of ongoing instability: at least one was clonal and therefore transmissible (Supplemental Figure 10). The presence of numerous blocks of ITS localized to only a few chromosomes is indicative of telomere fusion, occurring either as a result of mis-joining of two dysfunctional telomeres (telomere-telomere fusion), or fusion of a non-telomeric DSB end with an uncapped telomere (telomere-DSB

fusion) [44]. To ascertain the particular type of telomere fusion(s) generated in the *MMTV-Cre; Pot1a$^{\Delta/\Delta}$; p53$^{\Delta/\Delta}$* breast tumors, we performed Chromosome Orientation (CO)-FISH, a strand-specific cytogenetic methodology capable of distinguishing leading (C-rich) vs. lagging-strand (G-rich) telomeres [44, 45]. CO-FISH revealed that some of the ITS, including those present at centromeres of Robertsonian translocations, resulted from telomere-telomere fusions; i.e., red/green telomeric signals with no spaces in between (Figure 6B, Supplemental Figure 10A–C). However, the vast majority of ITS consisted of extensive blocks of G-rich or C-rich telomeric DNA interspersed with DAPI stained non-telomeric DNA (Figure 6B, Supplemental Figures 10A), a pattern most consistent with multiple telomere-DSB fusions (all red signals on one side and all green on the other). The source of the ITS could be either the ends of other chromosomes, or the result of amplification of the telomere fusion event. It is highly unlikely that the majority of ITS was derived from other chromosomal ends, as telomere-free ends were not increased in *MMTV-Cre; Pot1a$^{\Delta/\Delta}$; p53$^{\Delta/\Delta}$* breast tumors (Figures 6A, 6B, Supplemental Figures 10B, 10C). We have previously shown that fusion of telomeres devoid of mPOT1a promotes generation of dicentric chromosomes which form anaphase bridges [14]. Depending on how the anaphase bridge resolves during cytokinesis, breakage can occur within telomeric regions – or anywhere along the chromosome – setting up cycles of breakage-fusion-bridge (BFB) to fuel a highly unstable genome. Therefore, either a single telomere-telomere fusion, or a telomere-DSB fusion, could produce a dicentric chromosome, thereby triggering multiple rounds of BFB cycles and amplifying the telomeric signals.

To determine whether the extensive blocks of ITS observed in POT1 mutant tumors originated from a telomere-DSB fusion between two chromosomes or a telomere-telomere fusion between two sister chromatids (sister union), we employed Spectral Karyotyping (SKY) to identify individual mouse chromosomes. Not surprisingly, SKY revealed chromosomal duplications and multiple non-reciprocal translocations in breast tumor # 3327 (Figures 6C, 6D, Supplemental Figure 10D). More interesting was the observation that in this tumor, one of the amplified ITS regions was clonal and associated with chromosome 12, indicating that this particular ITS block likely resulted from a sister union that was subsequently amplified and duplicated via BFB cycles. We note that it was not possible to definitely ascertain the origin of the long telomeric blocks due to the repetitive (non-staining) nature of telomeric DNA. In support of repeated BFB cycles as the mechanism responsible for generating the aberrant ITS observed in *MMTV-Cre; Pot1a$^{\Delta/\Delta}$; p53$^{\Delta/\Delta}$* breast tumors, increased numbers of anaphase bridges and micronuclei were also observed (Figure 6E). Additionally, CO-FISH revealed an ~5-fold increase in the number of telomere sister chromatid exchanges (T-SCEs) [44] in these tumors (Figure 6F).

hPOT1 OB-folds protect newly synthesized telomeres from chromosome fusions

The aberrant chromosomes in *MMTV-Cre; Pot1a$^{\Delta/\Delta}$; p53$^{\Delta/\Delta}$* breast tumors bearing multiple blocks of ITS and increased T-SCEs observed are reminiscent of a small percentage of aberrant chromosomes showing similar phenotypes generated in the absence of the Apollo/SNM1b nuclease [45], suggesting that the cytogenetic aberrations might be associated with DNA replication. Immediately after DNA replication, leading-strand telomeres are initially blunt ended, while lagging-strand telomeres possess a short overhang due to placement

and/or removal of the terminal RNA primer. We have shown previously that the 5′ to 3′ Apollo/SNM1B exonuclease is recruited to telomeres to process the 5′ C-strands of leading-strand telomeres to generate the 3′ ss telomeric overhangs, to which POT1-TPP1 can bind and prevent leading-strand telomere fusion [46]. Apollo/SNM1B was not required at lagging strand telomeres because these already possess a minimal 3′ overhang after DNA replication, to which POT1-TPP1 can bind to and protect [46]. We used *Apollo/SNM1B* null MEFs to probe the protective functions of the POT1 OB-fold after DNA replication, postulating that an intact POT1 OB-fold is required for binding and protection of the 3′ ss overhangs of lagging-strand telomeres. Increased chromatid aberrations involving the lagging-strand telomere (as well as sister chromatid fusions) should be observed in *Apollo/SNM1B*$^{-/-}$ MEFs expressing mutant *hPot1*. On the other hand, the blunt ended leading-strand telomeres should be relatively unaffected by the presence of POT1 OB-fold mutations. To test this hypothesis, we expressed WT *mPot1a*, WT *mPot1b*, WT *hPOT1* with *hTPP1*, *mPot1a*^{F62A}, *mPot1b*^{F62A}, and *hPOT1* OB-fold mutants in *Apollo/SNM1B*$^{-/-}$ MEFs. Robust TIF formation was observed in cells expressing both mouse and human *Pot1* OB-fold mutants but not any of the WT *Pot1* alleles (Figures 7A, 7B). Greater than 90% of all chromosomal aberrations observed in *Apollo/SNM1B*$^{-/-}$ MEFs expressing mutant mouse and human *Pot1* DNA were end-to-end chromosome fusions with telomeres at fusion sites (Figures 7C, 7D, Supplemental Figures 11A, 11B). Aberrant chromosomes containing amplified blocks of ITS similar to those observed in the *MMTV-Cre; Pot1a*$^{\Delta/\Delta}$*; p53*$^{\Delta/\Delta}$ breast tumors were prominent in cells expressing all *Pot1* OB-fold mutants (Figures 7E, 7F, Supplemental Figure 11A, 11B). In addition, a small percentage of the telomere fusions were of the chromatid-type (Figure 7C, Supplemental Figure 11C, 11D). Unlike the relative paucity of lagging-strand chromatid fusions and sister fusions observed in *Apollo/SNM1B*$^{-/-}$ MEFs expressing vector control, expression of all *Pot1* OB-fold mutants resulted in increased number of chromatid fusions involving the lagging strand (Figure 7C, Supplemental Figure 11A, 11C, 11D). These results suggest that an intact POT1 OB-fold is required to protect the lagging-strand after DNA replication, and highlight the importance of POT1 OB-folds in protecting newly synthesized lagging-strand telomeres from triggering a DDR to prevent initiation of BFB cycles.

Discussion

Chromosomal structural aberrations are a hallmark of human cancers, with complex cytogenetic rearrangements leading to the amplification of oncogenes and deletion of tumor suppressors permissive for cancer initiation and progression [46]. These chromosomal aberrations could arise through the joining of chromosome ends lacking functional telomeres, resulting in the formation dicentric chromosomes that subsequently undergo BFB cycles to generate an unstable genome [47]. In mammalian cells, the p53 tumor suppressor integrates signals emanating from DNA DSBs to initiate cellular checkpoint responses and the induction of a tumorigenic barrier [48]. Consequently, mice bearing dysfunctional telomeres are usually resistant to tumor development due to the activation of p53-dependent cellular senescence and apoptosis programs [22, 49, 50]. In the absence of functional p53, telomerase deficiency [51] or deletion of shelterin components [14, 52] promotes telomere crisis and the formation of dysfunctional telomeres that are tumor promoting. *hPOT1* germline

mutations have been found in FM, glioma and cardiac angiosarcoma [36, 37, 53, 54], while somatic mutations are found in CLL [35]. However, whether these mutations function as driver or passenger mutations is not known.

Here, we report on the effect of *hPot1* OB-fold mutations in reconstituted cell lines and functional deletion of *mPot1a* in a mouse model of breast cancer. We found that expression of *hPot1* CLL and FM mutations generated uncapped telomeres, which were subsequently repaired via the A-NHEJ error-prone DNA repair pathway. While the hPOT1$^{\Delta OB}$ mutant [44] and hPOT1 OB-fold cancer mutations [35, 54] are thought to function as dominant negatives, we show that when expressed in a *mPot1a/mPot1b* null background, these mutants still negatively impact telomere functions. These results indicate that hPOT1 OB-fold mutants do not function as dominant negatives but rather as a null allele.

p53 plays a major role in preventing cancers bearing unstable telomeres. For example, telomeres lacking TRF2 initiates a DNA damage response that results in the activation of ATM, CHK2 and p53 to initiate apoptosis or cellular senescence. In the p53 heterozygous hematopoietic compartment, we found that expression of mutant *hPot1*^{Y223C} contributes to myeloproliferation and myeloid transformation. *hPot1*^{Y223C} expressing BM cells were able to engraft ICR-SCID mice and confer transplantable myloproliferative malignancy. The increased ability of hPOT1 mutant cells to proliferate into infiltrating malignant clones upon secondary re-transplantation is consistent with an enhanced ability in these cells for telomerase to lengthen telomeres during cellular replication. This notion is supported by the observation that human cancers bearing hPOT1 OB-fold mutations, as well as breast tumors derived from our *MMTV-Cre; Pot1a*$^{\Delta/\Delta}$*; p53*$^{\Delta/\Delta}$ mice, display increased telomere length [35–37, 54]. Since POT1 forms a heterodimer with TPP1, and together modulates telomerase processivity [8, 9], we postulated that the hPOT1 OB-fold mutations are unable to limit telomerase access to the ss telomeric DNA. Our *in vitro* primer extension assays revealed that despite the observation that all hPOT1 mutants failed to bind to ss telomeric DNA *in vitro*, only two hPOT1 mutants analyzed (hPOT1^{Y36N} and hPOT1^{Y89C}) were unable to inhibit telomerase activity as well as WT hPOT1. In contrast, all hPOT1 OB-fold mutants promoted telomere length elongation in HT1080 cells, suggesting that these mutations impacted upon the ability to negatively regulate telomerase access to telomeres. The discrepancy between the *in vitro* and *in vivo* findings are likely technical. Because the primer concentration (1 μM) used in the *in vitro* assay is ~100-fold greater than the dissociation constant of the POT1-DNA complex (~10 nM)[1155], it is reasonable that several of the DNA-binding defective hPOT1 mutants were still able to bind the DNA primer to inhibit telomerase activity.

Chromosomal fusions due to *mPot1a* deletion, or expression of *hPot1* OB-fold mutants, utilize A-NHEJ-mediated repair, in agreement with our previous data demonstrating that mPot1a/b normally represses A-NHEJ dependent DNA repair [25]. A-NHEJ uses regions of microhomology to align the DNA ends prior to Ligase 3 mediated end joining, and was initially thought to be a back-up repair pathway operating only in the absence of the classical, Ligase 4 dependent NHEJ. However, A-NHEJ appears to operate robustly even when C-NHEJ is functional [27, 39]. A-NHEJ is an inherently error-prone repair pathway and results in elevated genome instability. Better understanding of how the A-NHEJ repair

pathway is normally repressed at telomeres by the POT1 proteins and how it becomes activated in precursor cancer cells devoid of POT1 function to drive tumor initiation and progression, is therefore critically important. We show that in *MMTV-Cre; Pot1a$^{\Delta/\Delta}$; p53$^{\Delta/\Delta}$* breast tumors, massive blocks of amplified telomere signals are present on a few chromosomes. These cytogenetic aberrations are composed of both telomere-telomere and telomere-DSB fusions and likely arise from repeated rounds of BFB cycles. The generation of so many telomere-DSB fusions specifically localized to only a few chromosomes in the *MMTV-Cre; Pot1a$^{\Delta/\Delta}$; p53$^{\Delta/\Delta}$* breast tumors is reminiscent of chromothripsis, a unique pattern of genomic rearrangements confined to one or a few chromosomes found in some cancer cells [56]. Chromothrypsis has been postulated to arise from increased BFB cycles initiated by chromosomes bearing dysfunctional telomeres [56–59]. Sequestration of a broken acentric fragments into micronuclei (MN) and subsequent fragmentation and reassembly could result in the localization of cytogenetic aberrations to one or a few chromosomes [60]. However, while MN and anaphase bridges were both observed in *MMTV-Cre; Pot1a$^{\Delta/\Delta}$; p53$^{\Delta/\Delta}$* breast tumors, catastrophic shattering and random rejoining of chromosome fragments, a hallmark of chromothrypsis, CO-FISH revealed that the blocks of telomere-DSB fusions in these tumors appear not to be oriented randomly.

Finally, we have shown previously that repair of uncapped telomeres in *Apollo/SNM1B* null MEFs takes place immediately following DNA replication [45]. Our data reveal that the OB-folds of mPot1a and hPOT1 are required to mediate this protective function. POT1 OB-fold mutants fail to protect lagging-strand telomeres and initiate the formation of massive blocks of ITS resembling those observed in the *MMTV-Cre; Pot1a$^{\Delta/\Delta}$; p53$^{\Delta/\Delta}$* breast tumors. Since these chromosomal telomere fusion phenotypes arose through replication of chromatid-type telomere fusions formed during and/or after DNA replication, the generation of these ITS in the absence of POT1 function likely requires ongoing DNA replication. We have previously shown that in mice, mPOT1a recruits single-stranded binding protein 1 (SSB1) to telomeres to protect newly replicated telomeres [61]. We postulate that POT1 mutations or functional loss of POT1 prevents the recruitment of SSB1 to telomeres, resulting in increased telomere dysfunction during replication. Loss of telomere protective function generates both telomere-telomere and telomere-DSB fusions, thereby triggering multiple rounds of BFB cycles and amplifying the telomere signal. It is tempting to speculate that the failure of hPOT1 OB-fold mutations to modulate telomerase activity at telomeres in premalignant cancer cells, coupled with activation of a BFB cycle and enhanced A-NHEJ-mediated DNA repair, initiates rampant genome instability that favors tumor initiation and progression [62].

Materials and Methods

Generation of mouse models of cancer

To generate *MMTV-Cre; mPot1a$^{F/F}$; p53$^{F/F}$* mice, *MMTV-Cre* mice were crossed with *mPot1a$^{F/F}$* mice [14] to generate *MMTV-Cre; mPot1a$^{F/F}$* mice. *MMTV-Cre; mPot1a$^{F/F}$* mice were crossed with *p53$^{F/F}$* mice to generate *MMTV-Cre; mPot1a$^{F/F}$; p53$^{F/+}$* and *MMTV-Cre; mPot1a$^{F/F}$; p53$^{F/F}$* mice. *mPot1a$^{F/F}$* and *mPot1a$^{F/F}$; p53$^{F/F}$* mice were generated as controls. ICR-SCID were generated by standard matings. All mice were maintained according to the IACUC-approved protocols of Yale University.

Cell lines, plasmids and treatments

Mouse embryonic fibroblast cell lines, including *Ku70*$^{-/-}$, *Apollo/SNM1B*$^{-/-}$ *and CAG-Cre*^{ER}*; mPot1b*$^{-/-}$*; mPot1a*$^{F/F}$, were generated from the corresponding mice, immortalized with SV40-large T antigen (LT) and maintained in DMEM/high glucose media supplemented with 10% FBS. Human cell lines 293T, U2OS, HeLa, IMR90E6E7 and HT1080 were cultured in the same media. hPOT1 mutants were generated by site-directed mutagenesis (Stratagene) and constructed in retrovirus expression vectors pQCXIP-puro, MSCV-IRES-GFP or MSCV-IRES-Puro. All retrovirus was generated in 293T cell and infected target cells twice. Infection of mouse MEFs was performed with pCl-Eco help vector and infection of human cells was carried out with gal-pol and VSVG helper vectors. To efficiently express *hPot1* DNA constructs in MEFs, viruses expressing *hTpp1* was co-infected with viruses expressing *hPot1*. To delete *mPot1a* in *CAG-Cre*^{ER}*; mPot1b*$^{-/-}$*; mPot1a*$^{F/F}$ MEFs, cells were treated with 1μM of 4-hydroxy-tamoxifen for 24hr to delete the floxed *mPot1a* allele. 0.5ug/ml of PARP inhibitor PJ174 (CaliBiotech) was used to inhibit PARP activity.

DNA binding assay, Co-IP experiments and antibodies used

To examine whether mutant hPOT1 was able to bind to ss telomeric DNA *in vitro*, 293T cells expressing WT or mutant HA-hPOT1 were lysed and incubated in TEB_{150} buffer (50mM Hepes pH7.3, 150mM NaCl, 2mM $MgCl_2$, 5mM EGTA, 0.5% Triton-X-100, 10% Glycerol, proteinase inhibitors) overnight at 4°C with streptavidin-sepharose beads (Invitrogen) coated with biotin-Tel-G $(TTAGGG)_6$ oligo. Bound complexes were washed 3 times with same buffer. To probe for interactions between hTPP1 and hPOT1 mutants, 293T cells were transfected with pCl-Flag-hTPP1 and MSCV-IRES-GFP-hPOT1^{WT} or mutants. Lysates were incubated in TEB_{150} buffer and anti-Flag antibody cross-linked to agarose beads (Sigma, A2220) were used to Co-IP the Flag-hTPP1-HA-hPOT1 complex. After washing with TEB_{150} buffer, the beads were analyzed by immunoblotting. Antibodies used: anti-Flag M2 (Sigma F3165); anti-HA (Sigma H3663); anti-Myc (Millipore #05-724); anti-phospho-Chk1(cell signaling #2348); anti-phospho RPA2 (Bethyl A300-245A); anti-p53(Santa Cruz sc6243) and anti-p21 (Santa Cruz, sc6246).

Immunofluorescence and fluorescent *in situ* hybridization

Cells grown in chambers were fixed for 10 min in 2% (w/v) sucrose and 2% (v/v) paraformaldehyde at room temperature followed by PBS washes. Cells were blocked for 1 h in blocking solution (0.2% (w/v) fish gelatin and 0.5% (w/v) BSA in 1× PBS. The cells were incubated with primary antibodies ON at 4C at room temperature. After 0.1% Triton-PBS washes, coverslips were incubated with the appropriate Alexa fluor secondary antibody for 1 h followed by washes in 1XPBS with 0.1% Triton. IF-FISH was carried out as described [21] using a 5′-Cy3-OO-$(CCCTAA)_4$-3′ PNA telomere probe (PANAgene). DNA was counterstained with DAPI. Digital images were captured with a Nikon Eclipse 800 microscope utilizing an Andore CCD camera.

Chromosome analysis by Telomere PNA-FISH and CO-FISH

Cells were treated with 0.5 μg/ml of Colcemid for 4–7 h before harvest. Chromosomes were fixed and telomere PNA-FISH performed with a 5′-Cy3-OO-$(CCCTAA)_4$-3′ probe (PANAgene) as described [14, 63]. For CO-FISH, metaphase spreads were incubated sequentially with 5′-Cy3-OO-$(CCCTAA)_4$-3′ and 5′-FAM-CO-$(TTAGGG)_4$-3′ probes. Images were captured on a Nikon Eclipse 800 microscope and processed with MetaMorph Premier (Molecular Devices).

TRF Southern

25 μg of total genomic human DNA was digested with RsaI and HinfI overnight and separated in 0.8% agarose gel at 85V for 4.5 hr. The gels were dried and denatured with 0.5N NaOH, 1.5 M NaCl solution and neutralized with 3M NaCl, 0.5M Tris-Cl, pH 7.0. The pre-hybridized gel in Church mix (0.5M NaH_2PO_4, pH 7.2, 7% SDS) was hybridized with telomeric repeat oligonucleotide probe γ-^{32}P-$(CCCTAA)_4$ at 55° C overnight. Gels were washed with 4XSSC, 0.1% SDS buffer at 55 °C and exposed to Phosphorimager screens. For quantification of telomeric DNA, the gels were deprobed with re-denature and neutralization, and re-probed with γ-^{32}P-labelled Alu probes (GTGATCCGCCCGCCTCGGCCTCCCAAAGTG).

Telomerase activity assay

The direct primer extension assay to measure telomerase activity was performed based on published protocols [12]. Briefly, HEK 293T cells grown in wells of a 12-well plate were transfected with indicated plasmid DNA using Lipofectamine 2000 (Life Technologies) following the manufacturer's recommendations. 0.5 μg TERT-cDNA6/myc-HisC, 1.5 μg phTR-Bluescript II SK(+), 1 μg of HA-hPOT1-MSCV-IRES-GFP (wild type or mutant), and 0.5 ug of a plasmid expressing FLAG-tagged, full length (coding for amino acids 1–544) TPP1 were added per transfection. In control transfections where hPOT1 was omitted, 1 μg of empty vector was included. Two days after transfection, the cells were trypsinized, and the soluble contents were extracted using 40 μl CHAPS lysis buffer [64] followed by centrifugation (13,600 rpm, 10 min) to remove cell debris. The soluble fractions were flash frozen in liquid nitrogen and stored at −80°C. Telomerase reactions were carried out in 20 μl volumes containing: 50 mM Tris–Cl (pH 8.0), 30 mM KCl, 1 mM spermidine, 1 mM $MgCl_2$, 5 mM β-mercaptoethanol, 1 μM of primer a5 (TTAGGGTTAGCGTTAGGG), 500 μM dATP, 500 μM dTTP, 2.92 μM unlabelled dGTP, 0.33 μM radiolabeled dGTP (3000 Ci/mmol), and 5 μl of HEK 293T cell extracts at 30°C for 60 min. Reactions were quenched with buffer containing 100 μl of 3.6 M ammonium acetate, 20 μg of glycogen, and precipitated using ethanol. The pellets were resuspended in 10 μl H_2O and 10 μl of buffer containing 95% formamide, heated at 95°C for 10 min, and resolved on a 10% acrylamide, 7M urea, 1X TBE sequencing gel. Gels were dried, imaged on a phosphorimager (Storm; GE), and the data were analyzed using Imagequant TL (GE Life Sciences) software. Total activity in each lane was determined after application of the 'rolling ball' background correction.

Detection of telomerase RNA (TR) by RNA-FISH in HeLa cells

HeLa cells in 8-well chambers were transfected with 0.1μg of hTERT-cDNA6/myc-HisC and 0.3μg of phTR-Bluscript II SK(+). After 24hrs, cells were infected once with retrovirus expressing either WT hPOT1 or hPOT1 OB-fold mutants and maintained for 48hrs. Following PNA-FISH with Cy3-OO-$(CCCTAA)_4$, cells were incubated in prehybridization solution (0.1% Dextran sulfate, 1mg/ml of BSA, 2xSSC, 50% formamide, 0.5mg/ml spermidine DNA, 0.1mg/ml E.coli tRNA, 1mM RNase inhibitor VRC) at 37°C for 1hr, then hybridized with Cy5-TR RNA probes [65] (30ng/50ul probes in prehybridization solution) overnight at 37°C. The washing conditions are the same as described for PNA-FISH.

Immunoblot with telomerase extracts

3 μl each of soluble cell extracts prepared for the telomerase assay were subjected to immunoblotting using the mouse anti-FLAG M2-HRP antibody (Cat# A8592; Sigma; to detect FLAG-TERT and FLAG-TPP1) and the mouse anti-HA antibody (Cat# H3663; Sigma; to detect POT1).

Isolation of fetal liver and bone marrow cells

Fetal livers from E15.5 embryos were dissociated by passing through a 21-gauge needle. The cells were passed through 40μM cell strainers to generate single-cell suspensions. Red blood cells were removed with lysis buffer (3% acetic acid in methylene blue) (Stem Cell Technologies). Bone marrow cells were flushed from hind limb bones through a 21-gauge needle into HBSS+ (Hanks balanced salt solution (Invitrogen,), 2% FBS, and 10 mM HEPES.

Fetal liver and bone marrow transplantation

p53+/− fetal liver cells were incubated in IMDM media with 10% serum, concentrated retrovirus (MSCV-hPOT1-IRES-GFP and MSCV-hTPP1-IRES-NGFR) and 10 ng/ml IL-3/100 ng/ml stem cell factor (R&D systems). The efficiency of transduction by virus was determined on the basis of GFP and APC fluorescence by flow cytometry 24 h after a second round of infection. Cells expressing hTPP1 were identified with APC-anti-NGFR antibody (Biolegend). GFP and NGFR positive cells are around 30% of total. $1x10^6$ cells were injected retro-orbitally into 5.0-Gy-irradiated NOD-SCID recipient mice. To analyze the percentage of blood cell types, peripheral blood was analyzed. To obtain metaphases from BM cells, BM cells from transplanted SCID mice were suspended in DMEM with 10% serum at 37° C for 1 hr and treated with Colcemid for 2 hrs. Metaphases were prepared as described above. The transplantability of any malignancy generated was determined by injecting 1×10^6 bone marrow cells from mice with primary leukemia into sublethally irradiated mice and monitoring for the ability of this second transplantation to generate malignancy.

Histology and Flow cytometry analysis

Tissues were fixed in 10% formalin, paraffin embedded, sectioned at 5-μm thickness, and stained with H&E. To detect lineage markers on the bone marrow (BM) cells, 1×10^7 BM cells were centrifuged and re-suspended in 200 μl of $HBSS^+$ (Invitrogen), then stained for 15

minutes with antibodies. After staining, cells were washed, resuspended in $HBSS^+$, analyzed by flow cytometry (LSRII; BD) and stained with CD11b, CD4, CD8, B220, (eBioscience) conjugated with APC-Cy-7 (47–4317; eBioscience).

Supplementary Material

Refer to Web version on PubMed Central for supplementary material.

Acknowledgments

We wish to thank Dr. Asha Multani (MDACC, Houston, TX) for SKY analyses and Dr. James You (MDACC, Houston, TX) for histological analyses. We would like to thank the Chang lab for helpful suggestions. This work was supported by the NCI (RO1 CA129037, R01 CA202816, R21 CA200506 and R21 CA182280) and the CT Dept. of Public Health (15-002167) to S.C. Support for JN is from the NIH (NIH R00-CA-167644-03, NIH R01-AG050509 (J.N., co-investigator).

References

1. Greider CW. Telomere length regulation. Annual review of biochemistry. 1996; 65:337–365.
2. Verdun RE, Karlseder J. Replication and protection of telomeres. Nature. 2007; 447:924–931. [PubMed: 17581575]
3. Palm W, de Lange T. How shelterin protects mammalian telomeres. Annual review of genetics. 2008; 42:301–334.
4. Baumann P, Cech TR. Pot1, the putative telomere end-binding protein in fission yeast and humans. Science (New York, NY). 2001; 292:1171–1175.
5. Baumann P, Podell E, Cech TR. Human Pot1 (protection of telomeres) protein: cytolocalization, gene structure, and alternative splicing. Mol Cell Biol. 2002; 22:8079–8087. [PubMed: 12391173]
6. Liu D, Safari A, O'Connor MS, Chan DW, Laegeler A, Qin J, et al. PTOP interacts with POT1 and regulates its localization to telomeres. Nat Cell Biol. 2004; 6:673–680. [PubMed: 15181449]
7. Ye JZ, Hockemeyer D, Krutchinsky AN, Loayza D, Hooper SM, Chait BT, et al. POT1-interacting protein PIP1: a telomere length regulator that recruits POT1 to the TIN2/TRF1 complex. Genes & development. 2004; 18:1649–1654. [PubMed: 15231715]
8. Wang F, Podell ER, Zaug AJ, Yang Y, Baciu P, Cech TR, et al. The POT1-TPP1 telomere complex is a telomerase processivity factor. Nature. 2007; 445:506–510. [PubMed: 17237768]
9. Xin H, Liu D, Wan M, Safari A, Kim H, Sun W, et al. TPP1 is a homologue of ciliate TEBP-beta and interacts with POT1 to recruit telomerase. Nature. 2007; 445:559–562. [PubMed: 17237767]
10. Lei M, Podell ER, Baumann P, Cech TR. DNA self-recognition in the structure of Pot1 bound to telomeric single-stranded DNA. Nature. 2003; 426:198–203. [PubMed: 14614509]
11. Lei M, Podell ER, Cech TR. Structure of human POT1 bound to telomeric single-stranded DNA provides a model for chromosome end-protection. Nat Struct Mol Biol. 2004; 11:1223–1229. [PubMed: 15558049]
12. Nandakumar J, Bell CF, Weidenfeld I, Zaug AJ, Leinwand LA, Cech TR. The TEL patch of telomere protein TPP1 mediates telomerase recruitment and processivity. Nature. 2012; 492:285–289. [PubMed: 23103865]
13. He H, Multani AS, Cosme-Blanco W, Tahara H, Ma J, Pathak S, et al. POT1b protects telomeres from end-to-end chromosomal fusions and aberrant homologous recombination. The EMBO journal. 2006; 25:5180–5190. [PubMed: 17053789]
14. Wu L, Multani AS, He H, Cosme-Blanco W, Deng Y, Deng JM, et al. Pot1 deficiency initiates DNA damage checkpoint activation and aberrant homologous recombination at telomeres. Cell. 2006; 126:49–62. [PubMed: 16839876]
15. Hockemeyer D, Daniels JP, Takai H, de Lange T. Recent expansion of the telomeric complex in rodents: Two distinct POT1 proteins protect mouse telomeres. Cell. 2006; 126:63–77. [PubMed: 16839877]

16. Hockemeyer D, Palm W, Else T, Daniels JP, Takai KK, Ye JZ, et al. Telomere protection by mammalian Pot1 requires interaction with Tpp1. Nat Struct Mol Biol. 2007; 14:754–761. [PubMed: 17632522]
17. Denchi EL, de Lange T. Protection of telomeres through independent control of ATM and ATR by TRF2 and POT1. Nature. 2007; 448:1068–1071. [PubMed: 17687332]
18. Flynn RL, Centore RC, O'Sullivan RJ, Rai R, Tse A, Songyang Z, et al. TERRA and hnRNPA1 orchestrate an RPA-to-POT1 switch on telomeric single-stranded DNA. Nature. 2011; 471:532–536. [PubMed: 21399625]
19. Guo X, Deng Y, Lin Y, Cosme-Blanco W, Chan S, He H, et al. Dysfunctional telomeres activate an ATM-ATR-dependent DNA damage response to suppress tumorigenesis. The EMBO journal. 2007; 26:4709–4719. [PubMed: 17948054]
20. Thanasoula M, Escandell JM, Suwaki N, Tarsounas M. ATM/ATR checkpoint activation downregulates CDC25C to prevent mitotic entry with uncapped telomeres. The EMBO journal. 2012; 31:3398–3410. [PubMed: 22842784]
21. Palm W, Hockemeyer D, Kibe T, de Lange T. Functional dissection of human and mouse POT1 proteins. Mol Cell Biol. 2009; 29:471–482. [PubMed: 18955498]
22. Wang Y, Shen MF, Chang S. Essential roles for Pot1b in HSC self-renewal and survival. Blood. 2011; 118:6068–6077. [PubMed: 21948176]
23. Wang Y, Sharpless N, Chang S. p16(INK4a) protects against dysfunctional telomere-induced ATR-dependent DNA damage responses. The Journal of clinical investigation. 2013; 123:4489–4501. [PubMed: 24091330]
24. Rai R, Zheng H, He H, Luo Y, Multani A, Carpenter PB, et al. The function of classical and alternative non-homologous end-joining pathways in the fusion of dysfunctional telomeres. The EMBO journal. 2010; 29:2598–2610. [PubMed: 20588252]
25. Rai R, Li JM, Zheng H, Lok GT, Deng Y, Huen MS, et al. The E3 ubiquitin ligase Rnf8 stabilizes Tpp1 to promote telomere end protection. Nat Struct Mol Biol. 2011; 18:1400–1407. [PubMed: 22101936]
26. Sfeir A, de Lange T. Removal of shelterin reveals the telomere end-protection problem. Science (New York, NY). 2012; 336:593–597.
27. Bennardo N, Cheng A, Huang N, Stark JM. Alternative-NHEJ is a mechanistically distinct pathway of mammalian chromosome break repair. PLoS genetics. 2008; 4:e1000110. [PubMed: 18584027]
28. Badie S, Carlos AR, Folio C, Okamoto K, Bouwman P, Jonkers J, et al. BRCA1 and CtIP promote alternative non-homologous end-joining at uncapped telomeres. The EMBO journal. 2015; 34:828. [PubMed: 25766694]
29. Symington LS, Gautier J. Double-strand break end resection and repair pathway choice. Annual review of genetics. 2011; 45:247–271.
30. Ceccaldi R, Rondinelli B, D'Andrea AD. Repair Pathway Choices and Consequences at the Double-Strand Break. Trends in cell biology. 2016; 26:52–64. [PubMed: 26437586]
31. Fan J, Li L, Small D, Rassool F. Cells expressing FLT3/ITD mutations exhibit elevated repair errors generated through alternative NHEJ pathways: implications for genomic instability and therapy. Blood. 2010; 116:5298–5305. [PubMed: 20807885]
32. Tobin LA, Robert C, Nagaria P, Chumsri S, Twaddell W, Ioffe OB, et al. Targeting abnormal DNA repair in therapy-resistant breast cancers. Molecular cancer research : MCR. 2012; 10:96–107. [PubMed: 22112941]
33. He H, Wang Y, Guo X, Ramchandani S, Ma J, Shen MF, et al. Pot1b deletion and telomerase haploinsufficiency in mice initiate an ATR-dependent DNA damage response and elicit phenotypes resembling dyskeratosis congenita. Mol Cell Biol. 2009; 29:229–240. [PubMed: 18936156]
34. Quesada V, Conde L, Villamor N, Ordonez GR, Jares P, Bassaganyas L, et al. Exome sequencing identifies recurrent mutations of the splicing factor SF3B1 gene in chronic lymphocytic leukemia. Nature genetics. 2012; 44:47–52.
35. Ramsay AJ, Quesada V, Foronda M, Conde L, Martinez-Trillos A, Villamor N, et al. POT1 mutations cause telomere dysfunction in chronic lymphocytic leukemia. Nature genetics. 2013; 45:526–530. [PubMed: 23502782]

36. Robles-Espinoza CD, Harland M, Ramsay AJ, Aoude LG, Quesada V, Ding Z, et al. POT1 loss-of-function variants predispose to familial melanoma. Nature genetics. 2014; 46:478–481. [PubMed: 24686849]
37. Shi J, Yang XR, Ballew B, Rotunno M, Calista D, Fargnoli MC, et al. Rare missense variants in POT1 predispose to familial cutaneous malignant melanoma. Nature genetics. 2014; 46:482–486. [PubMed: 24686846]
38. Loayza D, Parsons H, Donigian J, Hoke K, de Lange T. DNA binding features of human POT1: a nonamer 5′-TAGGGTTAG-3′ minimal binding site, sequence specificity, and internal binding to multimeric sites. J Biol Chem. 2004; 279:13241–13248. [PubMed: 14715659]
39. Nussenzweig A, Nussenzweig MC. A backup DNA repair pathway moves to the forefront. Cell. 2007; 131:223–225. [PubMed: 17956720]
40. Guirouilh-Barbat J, Rass E, Plo I, Bertrand P, Lopez BS. Defects in XRCC4 and KU80 differentially affect the joining of distal nonhomologous ends. Proceedings of the National Academy of Sciences of the United States of America. 2007; 104:20902–20907. [PubMed: 18093953]
41. Boboila C, Jankovic M, Yan CT, Wang JH, Wesemann DR, Zhang T, et al. Alternative end-joining catalyzes robust IgH locus deletions and translocations in the combined absence of ligase 4 and Ku70. Proceedings of the National Academy of Sciences of the United States of America. 2010; 107:3034–3039. [PubMed: 20133803]
42. Lei M, Zaug AJ, Podell ER, Cech TR. Switching human telomerase on and off with hPOT1 protein in vitro. J Biol Chem. 2005; 280:20449–20456. [PubMed: 15792951]
43. Zhong FL, Batista LF, Freund A, Pech MF, Venteicher AS, Artandi SE. TPP1 OB-fold domain controls telomere maintenance by recruiting telomerase to chromosome ends. Cell. 2012; 150:481–494. [PubMed: 22863003]
44. Loayza D, De Lange T. POT1 as a terminal transducer of TRF1 telomere length control. Nature. 2003; 423:1013–1018. [PubMed: 12768206]
45. Lam YC, Akhter S, Gu P, Ye J, Poulet A, Giraud-Panis MJ, et al. SNMIB/Apollo protects leading-strand telomeres against NHEJ-mediated repair. The EMBO journal. 2010; 29:2230–2241. [PubMed: 20551906]
46. Artandi SE, DePinho RA. Telomeres and telomerase in cancer. Carcinogenesis. 2010; 31:9–18. [PubMed: 19887512]
47. McClintock B. The Stability of Broken Ends of Chromosomes in Zea Mays. Genetics. 1941; 26:234–282. [PubMed: 17247004]
48. Halazonetis TD, Gorgoulis VG, Bartek J. An oncogene-induced DNA damage model for cancer development. Science. 2008; 319:1352–1355. [PubMed: 18323444]
49. Rudolph KL, Chang S, Lee HW, Blasco M, Gottlieb GJ, Greider C, et al. Longevity, stress response, and cancer in aging telomerase-deficient mice. Cell. 1999; 96:701–712. [PubMed: 10089885]
50. Gonzalez-Suarez E, Samper E, Flores JM, Blasco MA. Telomerase-deficient mice with short telomeres are resistant to skin tumorigenesis. Nature genetics. 2000; 26:114–117. [PubMed: 10973262]
51. Artandi SE, DePinho RA. Mice without telomerase: what can they teach us about human cancer? Nature medicine. 2000; 6:852–855.
52. Martinez P, Thanasoula M, Munoz P, Liao C, Tejera A, McNees C, et al. Increased telomere fragility and fusions resulting from TRF1 deficiency lead to degenerative pathologies and increased cancer in mice. Genes & development. 2009; 23:2060–2075. [PubMed: 19679647]
53. Bainbridge MN, Armstrong GN, Gramatges MM, Bertuch AA, Jhangiani SN, Doddapaneni H, et al. Germline mutations in shelterin complex genes are associated with familial glioma. Journal of the National Cancer Institute. 2015; 107:384. [PubMed: 25482530]
54. Calvete O, Martinez P, Garcia-Pavia P, Benitez-Buelga C, Paumard-Hernandez B, Fernandez V, et al. A mutation in the POT1 gene is responsible for cardiac angiosarcoma in TP53-negative Li-Fraumeni-like families. Nat Commun. 2015; 6:8383. [PubMed: 26403419]

55. Nandakumar J, Podell ER, Cech TR. How telomeric protein POT1 avoids RNA to achieve specificity for single-stranded DNA. Proceedings of the National Academy of Sciences of the United States of America. 2010; 107:651–656. [PubMed: 20080730]

56. Stephens PJ, Greenman CD, Fu B, Yang F, Bignell GR, Mudie LJ, et al. Massive genomic rearrangement acquired in a single catastrophic event during cancer development. Cell. 2011; 144:27–40. [PubMed: 21215367]

57. Jones MJ, Jallepalli PV. Chromothripsis: chromosomes in crisis. Developmental cell. 2012; 23:908–917. [PubMed: 23153487]

58. Li Y, Schwab C, Ryan SL, Papaemmanuil E, Robinson HM, Jacobs P, et al. Constitutional and somatic rearrangement of chromosome 21 in acute lymphoblastic leukaemia. Nature. 2014; 508:98–102. [PubMed: 24670643]

59. Maciejowski J, Li Y, Bosco N, Campbell PJ, de Lange T. Chromothripsis and Kataegis Induced by Telomere Crisis. Cell. 2015; 163:1641–1654. [PubMed: 26687355]

60. Zhang CZ, Spektor A, Cornils H, Francis JM, Jackson EK, Liu S, et al. Chromothripsis from DNA damage in micronuclei. Nature. 2015; 522:179–184. [PubMed: 26017310]

61. Gu P, Deng W, Lei M, Chang S. Single strand DNA binding proteins 1 and 2 protect newly replicated telomeres. Cell Res. 2013; 23:705–719. [PubMed: 23459151]

62. Chang S. Cancer chromosomes going to POT1. Nature genetics. 2013; 45:473–475. [PubMed: 23619786]

63. Multani AS, Chang S. Cytogenetic analysis of telomere dysfunction. Methods Mol Biol. 2011; 735:139–143. [PubMed: 21461818]

64. Latrick CM, Cech TR. POT1-TPP1 enhances telomerase processivity by slowing primer dissociation and aiding translocation. The EMBO journal. 2010; 29:924–933. [PubMed: 20094033]

65. Abreu E, Terns RM, Terns MP. Visualization of human telomerase localization by fluorescence microscopy techniques. Methods in molecular biology (Clifton, NJ). 2011; 735:125–137.

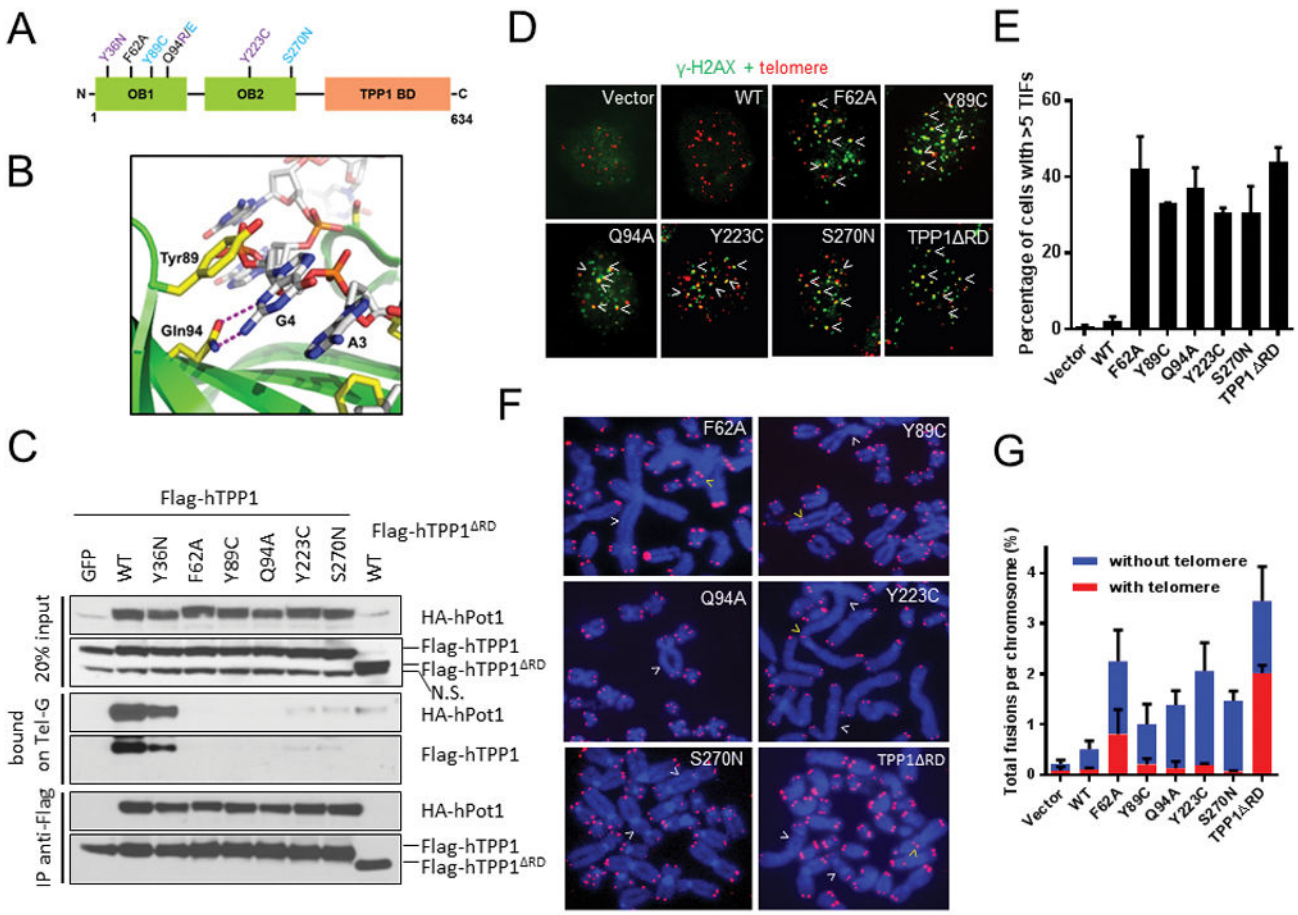

Figure 1. Human *Pot1* OB-fold mutants induce DNA damage response and chromosomal aberrations

A. Schematic of human POT1 OB-fold point mutations analyzed in this study. hPOT1 chronic lymphocyte leukemia (Y36N, Q94R, Y223C, in purple) and cutaneous familial melanoma (Y89C, Q94E, S270N, in blue) mutations are illustrated. The F62A mutation is illustrated in black. **B.** Ribbon diagram showing the electrostatic interactions between hPot1 Y89 and Q94 residues (yellow) and nucleotides A3 and G4 in telomeric DNA (red, white and blue). Protein-DNA intermolecular hydrogen bonds are illustrated as dotted pink lines. **C.** (top) DNA binding assay to determine the impact of hPOT1 mutations on interaction with ss telomeric DNA. WT or mutant *HA-hPot1* were co-expressed with *Flag-hTpp1* in 293T cells and incubated with biotinylated ss Tel G $(TTAGGG)_6$ oligonucleotides bound to streptavidin beads. Telomere bound hPOT1-hTPP1 was washed and eluted from the beads and hPOT1 detected by anti-HA immunoblotting. (bottom) Western blot of co-IP experiments to examine the interaction between WT and hPOT1 mutants with hTPP1. WT or mutant *HA-hPot1* were co-expressed with *Flag-hTpp1* in 293T cells. Protein complexes were immunoprecipitated with anti-Flag conjugated agarose beads, fractionated and detected with anti-HA antibody. Input represent for 10% lysate used for IP. **D.** γ-H2AX-positive foci at telomeres were used to monitor the number of dysfunctional telomere induced foci (TIFs) in U2OS cells infected with WT or mutant *hPot1*. Cells were immunostained with anti-γ-H2AX antibody (green), hybridized with Cy3-$(CCCTAA)_4$ probe to detect telomeres (red)

and DAPI (blue) to mark nuclei. *Tpp1*$^{\Delta RD}$ expression was used as a positive control for TIFs (arrowheads). **E.** Quantification of cells containing five or more γ-H2AX-positive TIFs in (**D**). Data represent the mean of three independent experiments; n>100 nuclei scored per experiments. Error bar represents standard error of the mean (s.e.m). **F.** Metaphase spreads were prepared from IMR90 cells expressing WT or mutant *hPot1* and telomere fusions visualized by telomere PNA-FISH (red) and DAPI (blue). White arrowheads point to fused chromosomes without telomeres at fusion sites, yellow arrowheads point to fusion sites with telomere signals. **G.** Quantification of telomere fusions from images shown in (**F**). Data are representative of the mean from three independent experiments and at least 35 metaphases. Error bars represent s.e.m.

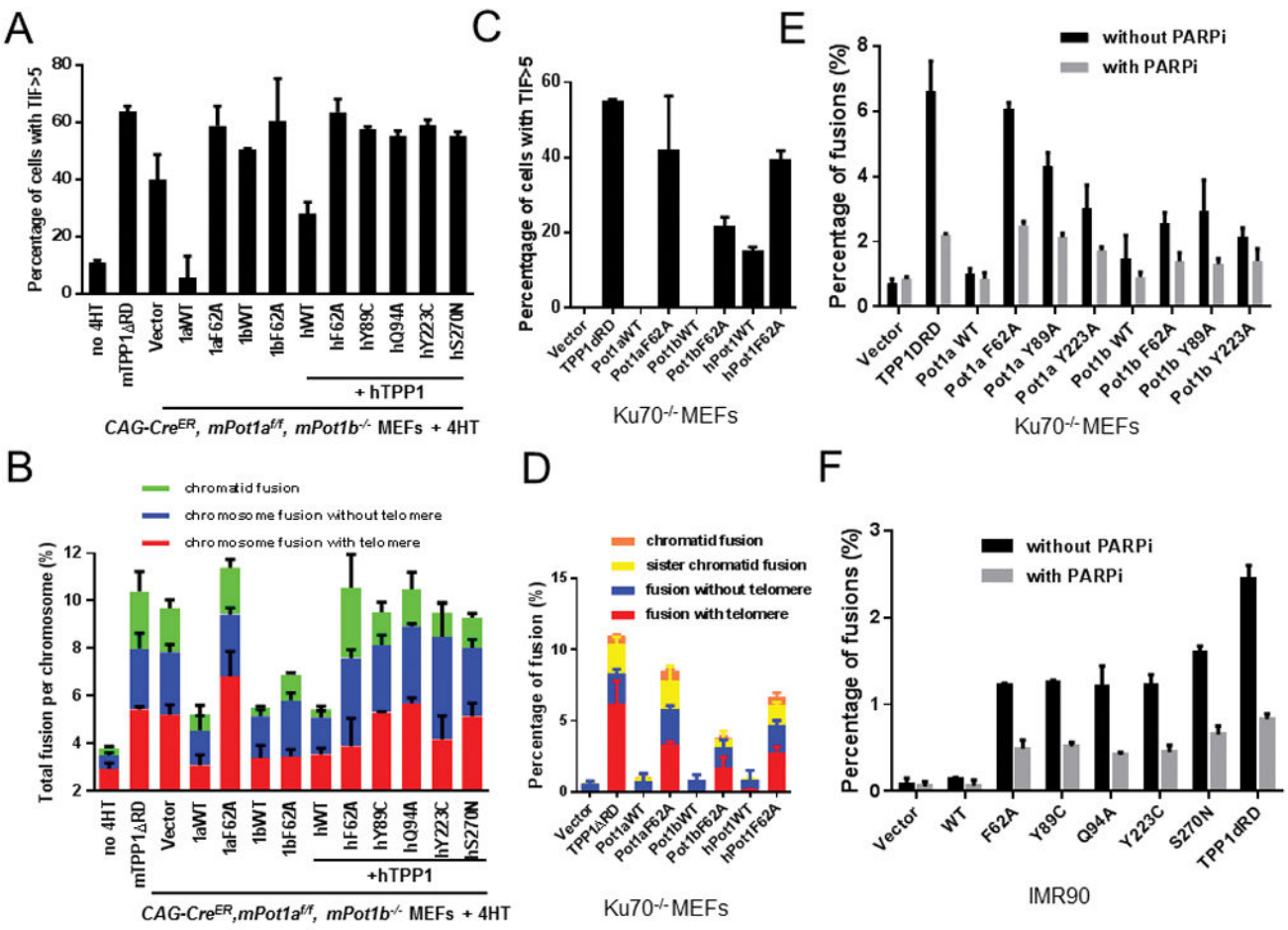

Figure 2. hPOT1 OB mutants promote A-NHEJ mediated chromosome fusions

A. Quantification of 4-HT treated *CAG-Cre^{ER}-mPot1a$^{F/F}$; mPot1b$^{-/-}$* MEFs expressing the indicated DNAs bearing five or more γ-H2AX-positive TIFs. Data represents the mean of three independent experiments; n>250 nuclei scored per experiments. Error bar represents s.e.m. **B.** Chromosome orientation (CO)-FISH analysis of metaphase spreads of 4-HT treated *CAG-Cre^{ER}-mPot1a$^{F/F}$; mPot1b$^{-/-}$* MEFs expressing the indicated DNAs. FAM-OO-$(TTAGGG)_4$ (green) was used to visualize the leading strand and Cy3-OO-$(CCCTAA)_4$ (red) used to visualize the lagging strand. A minimum of 120 metaphases from three independent experiments were scored for chromosome fusions with telomeres at fusion sites (red column), chromosome fusion without telomeres at fusion sites (blue column) and chromatid-chromatid fusions (green column). At least 35 metaphases were counted per experiment. Error bars represent s.e.m. **C.** Quantification of percentage of *Ku70$^{-/-}$* MEFs expressing the indicated DNAs bearing five or more γ-H2AX-positive TIFs. A minimum of 300 nuclei were scored in three independent experiments. Error bars represent s.e.m. **D.** Quantification of CO-FISH analysis of chromosomal fusions in (**C**). Fusions were scored as possessing telomeres at fusion sites (red column), fusions without telomeres (blue column), sister chromatid fusions (yellow column) and chromatid-chromatid fusions (orange column). Three independent experiments were performed, with a minimum of 40 metaphases were scored per experiment. Error bars represent s.e.m. **E.** Quantification of percentage *Ku70$^{-/-}$*

MEFs expressing the indicated DNAs with chromosomal fusions with or without treatment with 0.5 μM PARP1 inhibitor (PARP1i). A minimum of 40 metaphases were counted per experiment. **F.** Quantification of percentage of IMR90 cells expressing the indicated DNAs with chromosomal fusions with or without 0.5 μM PARP1 inhibitor (PARP1i). Two independent experiments were performed, with a minimum of 30 metaphases scored per experiment. Error bars represent s.e.m.

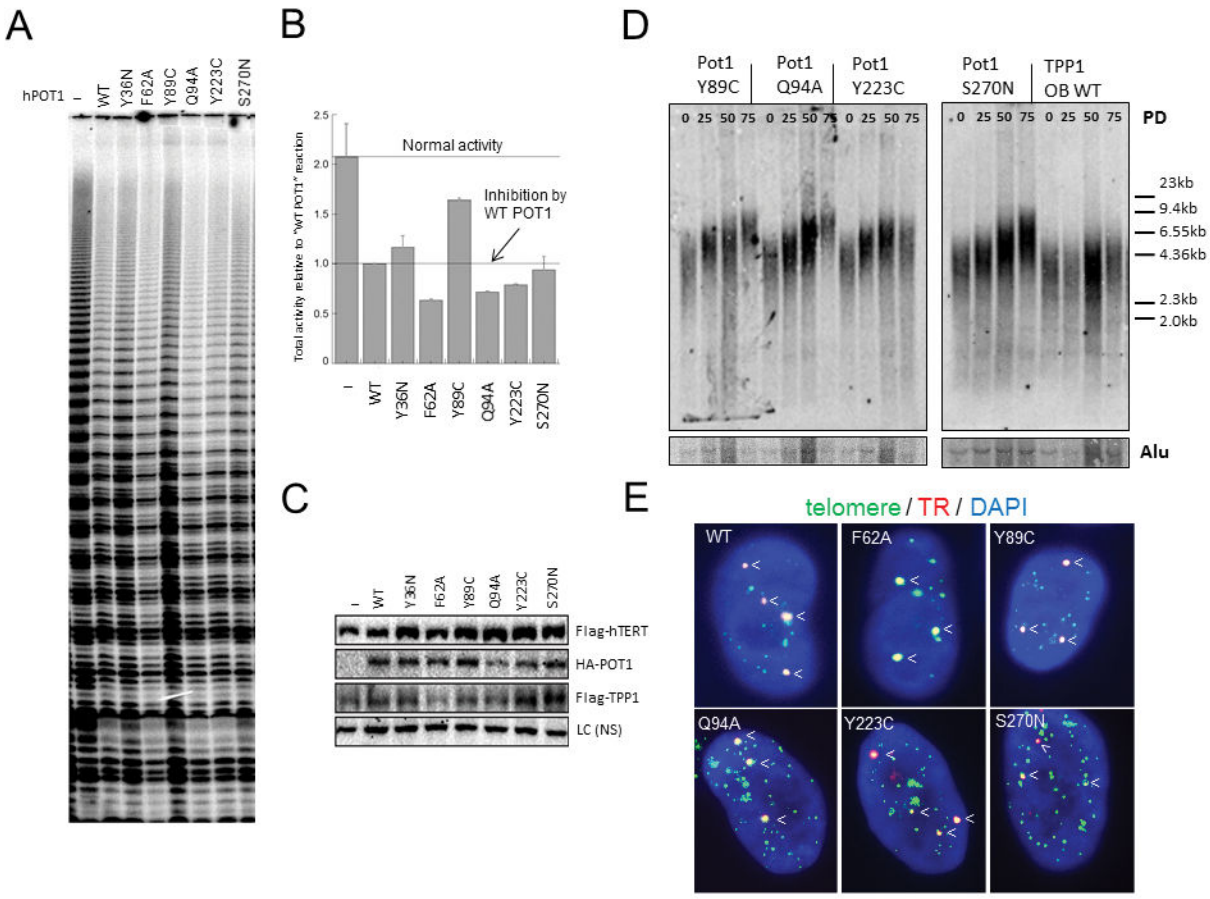

Figure 3. hPOT1 OB-fold mutants do not inhibit *in vitro* telomerase activity and promote telomere length elongation *in vivo*

A. Direct telomerase primer extension assays using lysates from HEK 293T cells co-transfected with TR, TERT, hPOT1 and hTPP1 plasmids. "-" indicates a transfection excluding the hPOT1-encoding plasmid. **B.** Quantification of telomerase activity data from two independent experiments. The horizontal lines show telomerase activity in the absence (upper line) versus presence (lower line) of wild-type HA-hPOT1 overexpression. All data were normalized to the telomerase activity of the reaction containing overexpressed wild-type HA-hPOT1. Error bars indicate the s.e.m. of experiments done in duplicate. **C.** Immunoblot of the telomerase extracts used in (A) probed with anti-FLAG (to detect TERT and hTPP1) and anti-HA (to detect hPOT1) antibodies. A non-specific (ns) band in the immunoblot appears at ~40 kDa with the anti-HA antibody. **D.** Telomere restriction fragment (TRF) Southerns to analyze telomere length in serially passaged HT1080 cells expressing the indicated DNAs. Genomic DNAs from cells isolated at population doublings (PD) 0, 25, 50 and 75 were fractionated with a clamped homogenous electric field (CHEF) gel. In-gel hybridization was performed using a radiolabeled $(CCCTAA)_4$ probe to detect total telomeric repeats. Re-hybridization with an Alu repetitive DNA probe was used to quantitate DNA loading. Molecular weight markers are on the right. **E.** Co-localization of human telomerase RNA (TR) on telomeres in HeLa cells overexpressing *hTert*, *hTR* and WT or mutant *hPot1*. Telomeres (green) were labeled with PNA probe Cy3-OO-$(CCCTAA)_4$ and

TR (red) was visualized by RNA-FISH with Cy5-TR probes. Nuclei were stained with DAPI (blue).

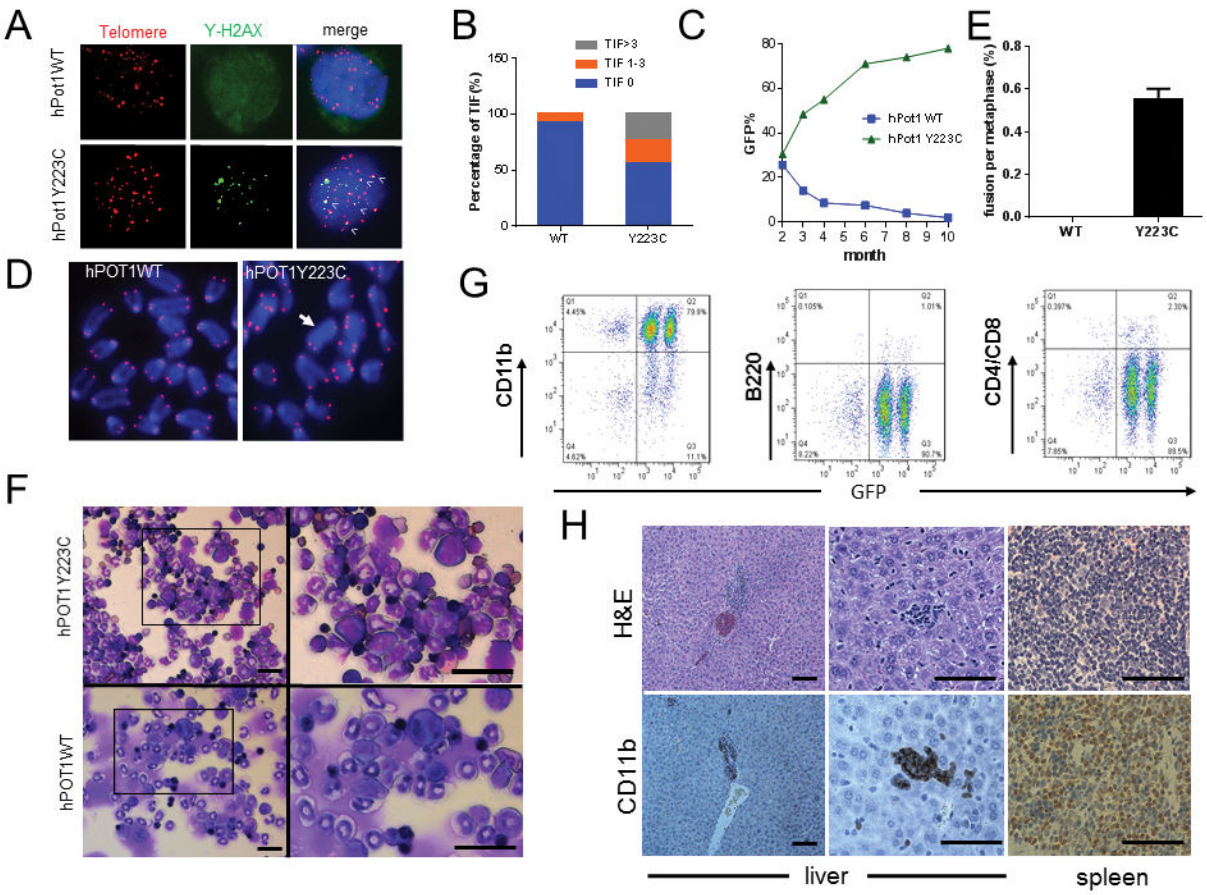

Figure 4. SCID mice reconstituted with hematopoietic cells expressing *hPOT1*^{Y223C} develop transplantable neoplasia

A. Representative TIF images of GFP-sorted *p53*$^{+/-}$ mouse fetal liver cells infected with MSCV-hPot1^{WT}-IRES-GFP or MSCV-hPot1^{Y223C}-IRES-GFP. Cells were stained with anti-γ-H2AX antibody (green), telomere PNA-FISH probe [Cy3-OO-(CCCTAA)$_4$ (red)] and DAPI (blue). **B.** Quantification of percentage sorted GFP$^+$ cells displaying γ-H2AX-positive TIFs. Increased percentage of cells displaying >3 TIFs per nucleus was detected in fetal cells expressing the *hPot1*^{Y223C} mutant compared with WT *hPot1* (P<0.001). A total of 150 nuclei were scored per genotype in two independent experiments. **C.** The percentages of hPOT1^{WT}-GFP$^+$ and hPOT1^{Y223C}-GFP$^+$ cells in the peripheral blood of transplanted ICR-SCID mice were monitored over time by flow cytometry. **D.** Telomere PNA-FISH of metaphase spreads showing an end-to-end chromosome fusion (arrow) only in bone marrow (BM) cells derived from ICR-SCID mice reconstituted with hPOT1^{Y223C}-GFP$^+$ fetal liver cells. **E.** Quantification of chromosome fusions in (D). A minimum of 25 metaphases were analyzed in two independent experiments. Error bars represent s.e.m. **F.** Cytospins of BM cells derived from mice reconstituted with fetal liver cells expressing hPOT1^{WT}-GFP$^+$ or hPOT1^{Y223C}-GFP$^+$ were stained with Wright-Giemsa. Myeloid dysplasia was detected with a neutrophil predominance and a prominent myeloid left shift. Higher magnification of boxed areas is shown in the right panels. Scale bars: 20 microns. **G.** FACS profiles of BM cells from ICR-SCID mouse expressing the *hPot1*^{Y223C} mutation. Note the substantial

increase in the $CD11b^{+}$, GFP^{+} myeloid subpopulation. **H.** H&E and immunohistological analysis of livers and spleens from recipient SCID mice after a second round of BM transplantation with BM cells from ICR-SCID mice expressing the *hPot1*^{Y223C} mutation. Nests of malignant infiltrating hematopoietic cells were detected by both H&E (upper panels) and anti-CD11b immunostaining (lower panels), a marker for myeloid cells. Scale bars: 20 microns.

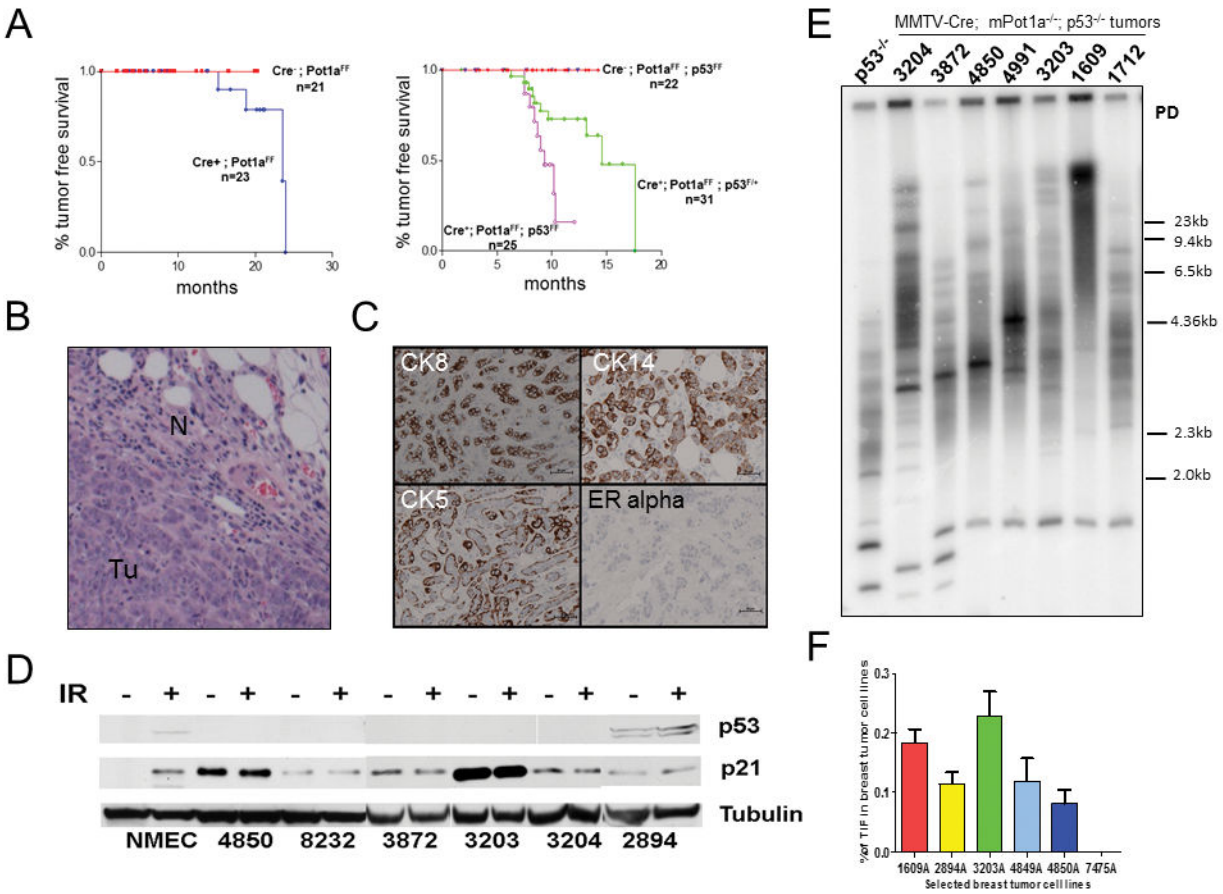

Figure 5. Characterization of breast cancers derived from *MMTV-Cre, mPot1a$^{F/F}$, p53$^{F/F}$* mice

A. Kaplan-Meier survival curve of mice of the indicated genotypes. Number of mice analyzed is indicated. **B.** H&E analysis of invasive cancer (Tu) and normal tissue (N) from a *MMTV-Cre, mPot1a$^{F/F}$, p53$^{F/F}$* mouse. **C.** Immunostaining of paraffin-embedded sections from a *MMTV-Cre, mPot1a$^{\Delta/\Delta}$, p53$^{\Delta/\Psi}$* breast tumor with epithelial specific markers CK5, CK8, CK14 and ER-α. **D.** Western analysis of *MMTV-Cre, mPot1a$^{\Delta/\Delta}$, p53$^{\Delta/\Delta}$* breast tumor cell lines for the functional status of p53. Tumor cells were either untreated (-) or irradiated (+) with 10Gy IR and lysates were probed with antibodies against p53 and p21. Mouse tumor numbers are indicated. NMEC: normal mammary epithelial cells. **E.** TRF-Southern analysis of total telomere lengths in breast tumors from *MMTV-Cre, mPot1a$^{F/F}$, p53$^{F/F}$* mice. Genomic DNAs from tumors were fractionated with a clamped homogenous electric field (CHEF) gel. In-gel hybridization was performed using a radiolabeled $(CCCTAA)_4$ probe to detect total telomeric repeats. MW markers are on the right. Tumor numbers are indicated. **F.** Percentage of γ-H2AX positive TIFs in *MMTV-Cre, mPot1a$^{\Delta/\Delta}$, p53$^{\Delta/\Delta}$* breast tumor cell lines.

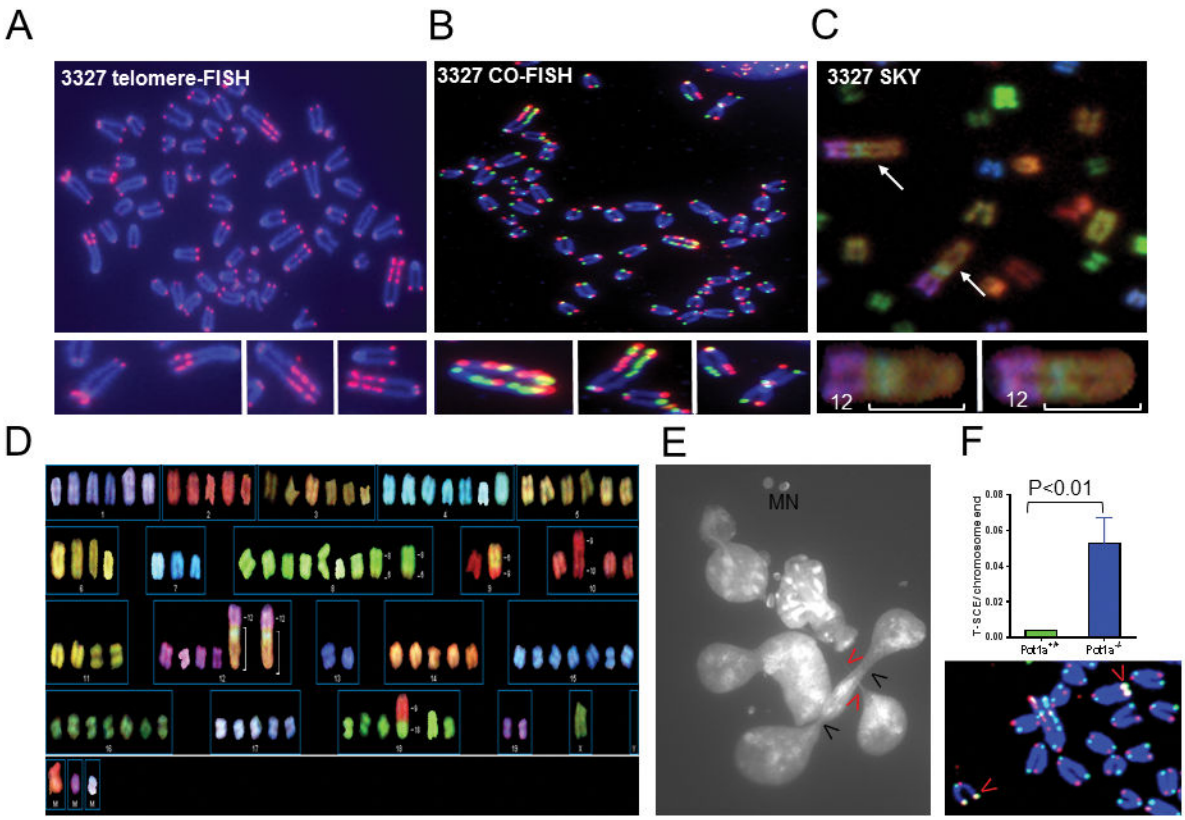

Figure 6. Amplification of telomere fusion events in *MMTV-Cre, mPot1a*$^{\Delta/\Delta}$, *p53*$^{\Delta/\Delta}$ breast tumors

A, B. Metaphase chromosome spreads from a representative *MMTV-Cre, mPot1a*$^{\Delta/\Delta}$, *p53*$^{\Delta/\Delta}$ breast tumor (3327) illustrating rampant chromosomal instability. Several chromosomes with large blocks of ITS detected by telomere PNA-FISH (A) or CO-FISH (B) are shown. For CO-FISH, green signals represent FAM-OO-$(TTAGGG)_4$ detection of leading-strand telomeres, and red signals Cy3-OO-$(CCCTAA)_4$ detection of lagging-strand telomeres. Both amplified telomere-telomere and telomere-DSB fusions are observed, as well as Robertsonian translocation with telomere-telomere fusion at centromeres. **C**. Chromosome translocations (arrows) analyzed by SKY. Two marker chromosomes containing ITS (bracket) and portions of chromosome 12 are shown. **D.** SKY karyogram of the *MMTV-Cre, mPot1a*$^{\Delta/\Delta}$, *p53*$^{\Delta/\Delta}$ 3327 breast tumor. Chromosome duplications and non-reciprocal translocations (t6;9, t9;10, t8,6, t9;18) are detected. Note that the ITS blocks (brackets) are fused to chromosome 12. **E**. Anaphase bridges (black and red arrowheads) and micronuclei (MN), indicative of chromosomal fusion/dicentric formation, in a representative breast tumor. **F**. Increased frequencies of telomere-sister chromosome exchange (T-SCE) were also observed in *MMTV-Cre, mPot1a*$^{\Delta/\Delta}$, *p53*$^{\Delta/\Delta}$ breast tumors.

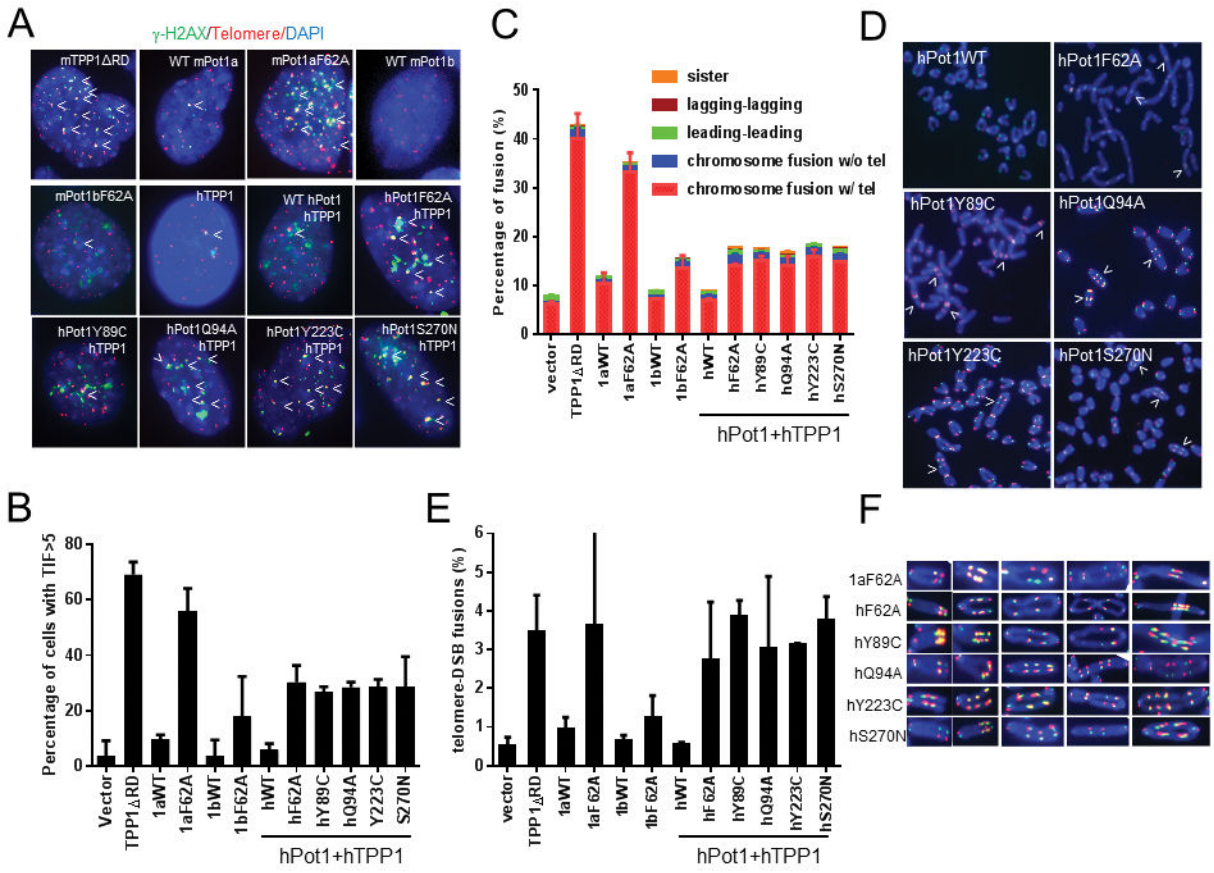

Figure 7. *hPot1* OB-fold mutants generate telomere-DSB fusions in in *Apollo*$^{-/-}$ MEFs

A. TIF formation in *Apollo*$^{-/-}$ MEFs expressing *mPot1a*^{F62A} or *hPot1* OB-fold mutants with *hTpp1*. **B**. Quantification of percentage of cells with >5 γ-H2AX positive TIFs in (A). Data represents the mean of three independent experiments; n>100 nuclei per experiments. Error bars represent s.e.m. **C.** Quantification of the percent of total chromosome and chromatid fusions observed in *Apollo*$^{-/-}$ MEFs expressing WT *mPot1a*, *mPot1b*, *mPot1a*^{F62A}, *mPot1b*^{F62A}, WT *hPot1* or *hPot1* mutants. Metaphase chromosomes were analyzed by CO-FISH; FAM-OO-$(TTAGGG)_4$ (green) visualizes the leading-strand telomere, and Cy3-OO-$(CCCTAA)_4$ (red) the lagging-strand telomere. Three independent experiments were scored for the presence of fusion sites with telomeres (red column), without telomeres (blue), leading-leading strand chromatid fusions (green), lagging-lagging strand chromatid fusions (brown) and sister chromatid fusions (orange). At least 35 metaphases were scored per experiment. Error bars represent s.e.m. **D.** Representative images of the types of telomere fusions in *Apollo*$^{-/-}$ MEFs expressing the indicated DNAs. Aberrant chromosomes are indicated by arrowheads. **E.** Quantification of the percentage of telomere-DSB fusions observed in *Apollo*$^{-/-}$ MEFs expressing the indicated DNAs. Data represents the mean of three independent experiments; n>40 metaphases analyzed per experiments. Error bar represents s.e.m. **F.** Examples of telomere-telomere and telomere-DSB fusions observed in *Apollo*$^{-/-}$ MEFs expressing *mPot1* or *hPot1* OB-fold mutants. CO-FISH was used to label telomere ends; FAM-OO-$(TTAGGG)_4$ (green) visualized leading-strand telomeres and Cy3-

OO-$(CCCTAA)_4$ (red) the lagging-strand telomere. Note: Both telomere-telomere and telomere-DSB fusions are shown.